Study of the Behavior of a Commercial Scale Inhibitor on Silica Sand

by

Victor O. Vaca Bustamante

B. S. in Petroleum Engineering, University of Kansas, 2006

Submitted to the graduate degree program in Chemical and Petroleum Engineering and the Graduate Faculty of the University of Kansas in partial fulfillment of the requirements for the Degree of Master of Science.

Thesis Committee:

_____

Dr. G. Paul Willhite, Chair

_____

Dr. Stephen J. Johnson

_____

Dr. Jyun-Syung Tsau

Date Defended: June 11, 2010

Acceptance Page

The Thesis Committee for Victor Vaca Bustamante certifies

that this is the approved version of the following thesis:

Study of the Behavior of a Commercial
Scale Inhibitor on Silica Sand

Thesis Committee:

_____

Dr. G. Paul Willhite, Chair

_____

Dr. Stephen J. Johnson

_____

Dr. Jyun-Syung Tsau

Date Approved: December 14, 2010

Acknowledgments

This work would not have been possible without my parents' uninterrupted encouragement. I am infinitely grateful for their love and support.

I would like to extend my deepest and sincere appreciation to my advisors Professor Paul Willhite and Professor Jenn-Tai Liang for their constant guidance during the course of my research. Their support and recommendations are greatly appreciated.

A special gratitude goes to Dr. Stephen J. Johnson, who has been a great mentor throughout my research. His teachings and his constant guidance are immensely appreciated. He diligently provided me support in the lab and with my writing. I am sincerely grateful for his patience and insightful recommendations.

I would like to thank Dr. Jyun-Syung Tsau for serving on my dissertation committee. Also, I would like to thank Professor Don W. Green for his continuing support and kind mentoring. Special thanks go to Dr. Sheng-Xue Xie and Dr. Karen Peltier for their assistance in operating the laboratory equipment and technical advice. In addition, I would like to thank Mr. Scott Ramskill for his valuable cooperation in designing, constructing and operating the laboratory. His assistance was of vital importance for my laboratory work. For that, I am grateful. Mr. Jim Pilch helped me earlier in the project, and I would like to acknowledge his help. I also thank Ms. Mayumi Crider, Ms. Maxine Younes and all other TORP staff members and friends. I would like to demonstrate my gratitude to Dr. Mike Michnick. His perspicacious recommendations and constant assistance is appreciated. In addition, I appreciate the financial aid provided by TORP.

Finally, I would like to address special gratitude to my girlfriend, Danica May. Her patience and support were crucial for the culmination of this thesis.

Table of Contents

List of Figures

List of Tables

Chapter 1

Introduction

1.1 Scale Problem

Oil and gas production from underground reservoirs are frequently associated with production of water. Mineral deposition or scale formation in rock pores, tubing and downhole equipment occurs due to precipitation of inorganic minerals in the presence of water. In addition, the life cycle of a reservoir influences scale formation, as well as the geographical location (onshore or offshore), temperatures and pressures. There are two distinct mechanisms for scale deposition to occur, pressure loss affecting dissolved carbonate equilibrium and the mixing of incompatible brines that yields sulfate scales.

The supersaturation of the local environment with an inorganic salt results in mineral deposition. Formation damage, tubular plugging and submersible equipment failure result in reduced oil and gas flow and may even cause abandonment of the well. This problem causes a considerable economic impact, estimated at more than USD 1.4 billion each year [1].

1.2 Use of Scale inhibitors

There are several types of inorganic scale, the most damaging and most expensive to handle is sulfate scale. It forms due to the co-production of barium-rich formation or aquifer water, with injected seawater in the case of a waterflood, which is rich in sulfate. The resulting mixture is highly supersaturated with respect to barium sulfate due to its considerably low

solubility (K_{sp} =1.07 x 10^{-10} mol.dm^3) [2]. Barite and other sulfates are insoluble even in concentrated acids and can only be removed by using expensive chelators such as EDTA (ethylenediamine-tetra-acetic acid), or by tedious and expensive mechanical methods such as milling or water jetting [3]. The most economically feasible method to combat scale is prevention by the use of scale inhibitors. This is achieved by the injection of crystal growth inhibiting water soluble chemicals into the formation through a production well in a squeeze treatment. Once the chemicals are deployed in the rock matrix, adsorption takes place. When production is brought back after a squeeze treatment, the inhibitor desorbs from the rock grains and remains dissolved in the produced waters, which prevents scaling until the concentration falls too low to be effective. The amount of time that requires for the inhibitor concentration to fall below this minimum inhibitor concentration (MIC) is called the squeeze lifetime.

1.3 Objective and Scope

Squeeze treatments are expensive [1]; in addition to the cost of the chemicals and injection, the well is usually shut-in for several days causing considerable economic loss [18]. Therefore, the ultimate concern of the operator is to have long squeeze lifetimes in order to minimize the number of treatments, thus reducing the cost. The objective of this thesis was to study the adsorption of the commercial scale inhibitor SI onto silica sand. By investigating this intrinsic phenomenon, an optimized squeeze treatment can be designed in the future, thus saving money to the operator. This objective was pursued by the investigation of the behavior and interaction of the scale inhibitor SI, field brine and synthetic seawater (SW) under reservoir conditions via porous media displacement experiments. The scale inhibitor adsorption tests were done at 70 ^{o}C.

Chapter 2

Literature Review

In this chapter a review of the nucleation and crystal growth theories of major relevance to this investigation is presented. Section 2.1 covers the mechanisms and driving forces of scale formation. Section 2.2 describes the physical phenomenon of crystal growth and how its understanding is crucial to prevent scale formation. Then fundamental aqueous thermodynamics is reviewed in Section 2.3, and Section 2.4 describes the mechanisms of scale inhibition for both nucleation and crystal growth. Adsorption of scale inhibitor on barium sulfate and on silica is discussed and results from other authors are revised.

Most of the literature review discusses the efficiency and adsorption of phosphonate scale inhibitors, which are the most common inhibitors used in the oil and gas industry. This includes laboratory studies on static and dynamic efficiency tests that address pH, molecular weight and calcium concentration as factors that affect adsorption.

2.1 Scale formation: Crystallization

Two conditions must exist for scale to form: a supersaturated aqueous environment, and the rate of formation of scale being greater than the residence time of the water at near wellbore and downhole equipment. When a critical surface is present under those conditions, scale becomes a problem. Therefore, conditions that cause supersaturation, rate of crystal growth, and surface factors are crucial for assessing scale damage and prevention. Some of these conditions

are temperature or pressure change, pH shift, or contact between incompatible waters. Scale formation occurs in two stages, nucleation and crystal growth.

Nucleation is the first step of the scale formation process, when several thousand of molecules appear as unstable clusters of atoms [3]. Changes in concentrations of ions in supersaturated solutions result in the formation of small seed crystals. These crystals consequently grow when ions absorb onto uneven crystal surfaces. The main difference between homogenous and heterogeneous nucleation is that the first one occurs in pure solutions with no solids present, and the latter occurs when nuclei form on solid material already present, e.g. pipe surface roughness or existing scale. The energy for seed crystal growth is driven by a reduction in the surface free energy of the crystal [1]. Theoretically there are two free energy terms that contribute to precipitation, the one that is responsible for the creation of new surface (which is positive) namely ΔG_s, and the one that represents molecules' stabilization in the bulk crystal (which is negative), ΔG_v. In homogenous nucleation, the total free energy change that occurs as a result of small clusters formation is unfavorable, therefore nuclei must reach a critical size of radius r_c before crystallization occurs [3]. Figure 2.1 describes how the reduction of surface free energy is responsible for seed crystal growth. In other words, the less the surface free energy of crystal, the more energy for a new seed crystal to grow will exist. Therefore, the resultant free energy term will be negative as new surface for scale to grow forms.

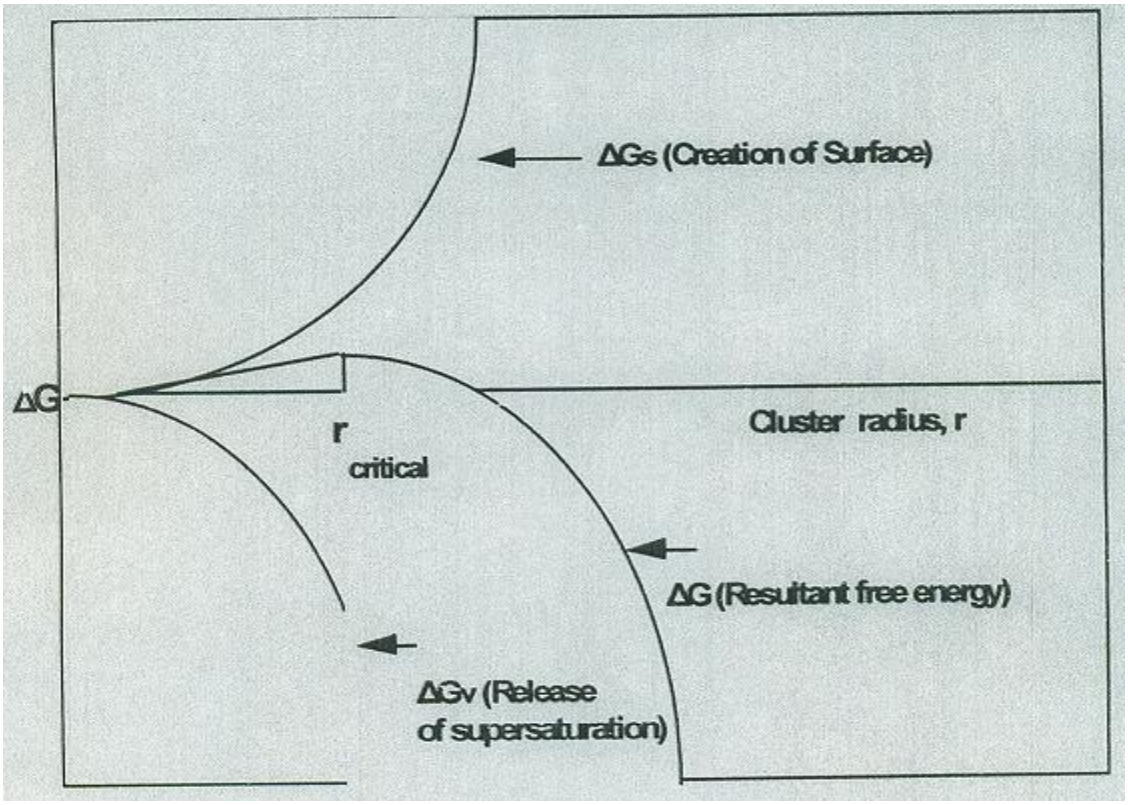

Figure 2. 1 Free Energy dependency on the crystal radius (Laing, 2006)

For heterogeneous nucleation, a non-uniform pipe surface, rock matrix or existing scale is already present and provides a pre-existing surface for nucleation; therefore, the free energy is reduced and precipitation occurs more easily. Figure 2.2 describes homogenous and heterogeneous nucleation processes visually.

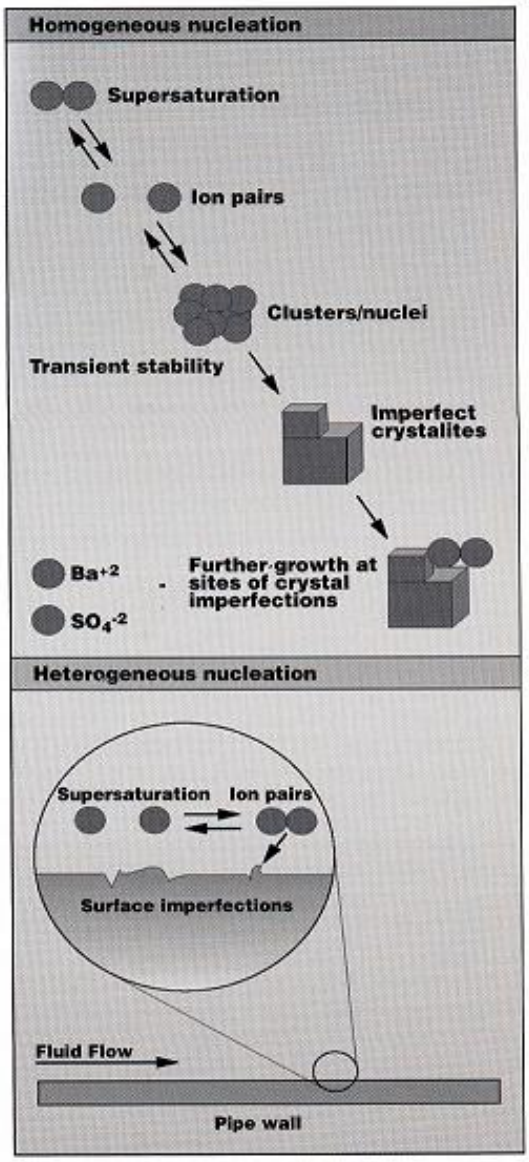

Figure 2. 2 Process of Scale Formation (Frenier et al. 2008)

2.2 Crystal Growth

The second step in scale mineral formation is crystal growth, which occurs after nucleation. Nuclei grow into larger stable crystals by adsorbing dissolved molecules from the supersaturated solution. There are three growth mechanisms, spiral growth, birth & spread and roughened growth. The spiral growth mode is dominant at low supersaturation and occurs where non-uniformity of the surface exists, forming a monomolecular step which may be straight or "kinked" [3]. These kinks are active growth sites because ions and molecules attaching to a kinked step interact with two or three layers rather than just one below, in the case of flat surface adsorption. This mechanism was proposed by Frank et al in 1949, and is known as the BCF (Burton, Cabrera and Frank) theory (Burton et al. (1951) cited in Laing [3]). Birth & spread occurs at moderate supersaturation, and it does not depend on surface non-uniformities or defects. Nucleation takes place on the surface of a growing crystal and with time and the right conditions it expands out from the nucleus to form a new layer. Each layer depends on the formation of a nucleus on its surface and more than one nucleus can form on the surface and spread out to meet another. Therefore, nucleation is the rate determining step in the birth & spread mechanism. Roughened growth mechanism occurs at high supersaturation. Crystal growth by this mechanism takes place in a roughened surface because of the existing active growth sites. Figure 2.3 illustrates the nature of "kinks" and how they become active growth sites.

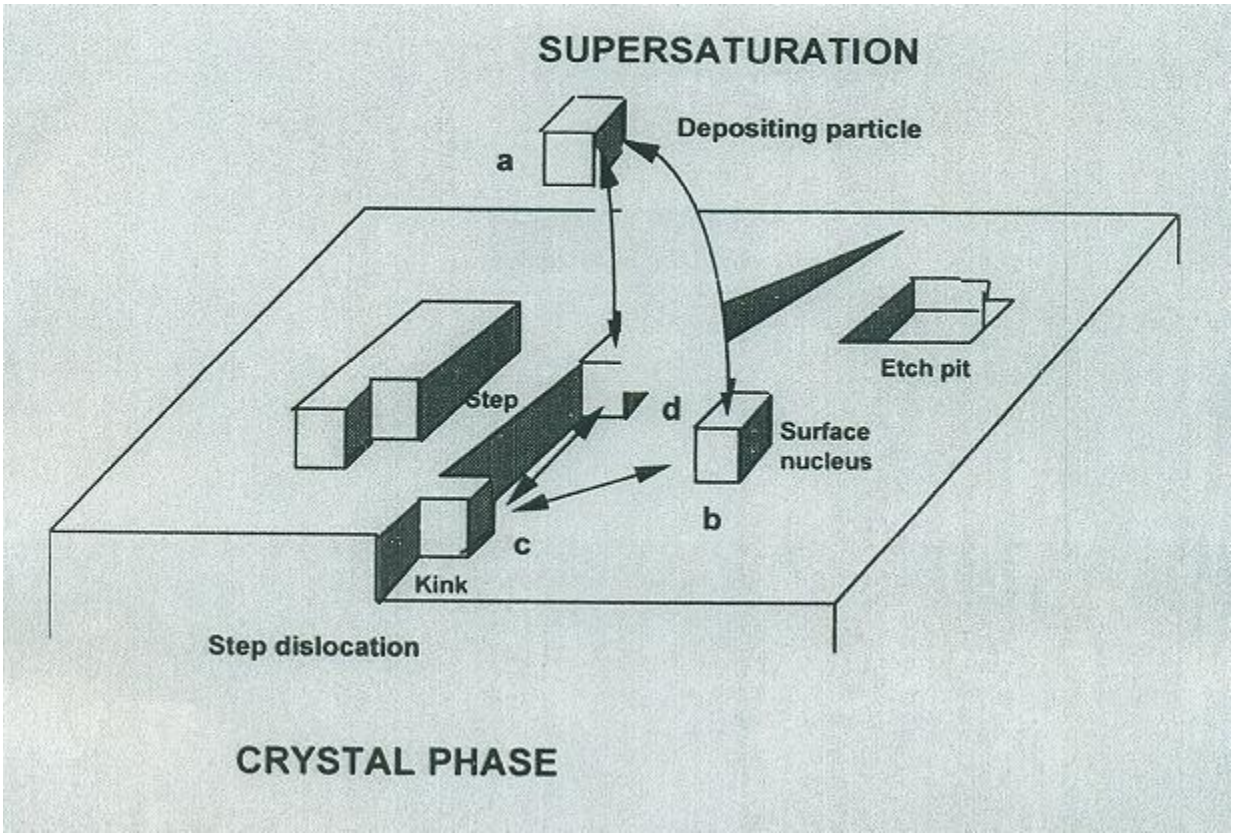

Figure 2. 3 Schematic of step growth on a crystal face (Laing, 2006)

2.3 Thermodynamics

The interruption in chemical equilibrium in an aqueous system is partly responsible for scale formation. When chemical equilibrium exists in an aqueous system, two or more reactions take place dynamically and they are opposite from each other (i.e. rate of formation of products – rate of formation of reactants is equal to zero). Equilibrium constants are used to relate the amounts of reactants and products at equilibrium [1]. For example, in an ideal chemical system where A and B are reactants and C and D are products, the equilibrium constant for the system can be expressed in terms of concentration:

$$K_{eq} = \frac{[C]^c[D]^d}{[A]^a[B]^b} \quad \text{..... (2.1)}$$

Where K_{eq} is the equilibrium constant, and [C] and [D] represent concentrations of the species C and D. K_{eq} can also be written as a function of free energy change for the reaction (ΔG^0) as shown in Equation 2.2. Also, based on the discussion from Section 2.1, reduction of the surface free energy of the crystal is responsible for crystal growth.

$$K_{eq} = \exp\left(\frac{-\Delta G^0}{RT}\right) \quad \text{..... (2.2)}$$

Where R is the gas constant which is equal to 8.3144 [2] and T is the temperature in Kelvin. K_{eq} is a function of only temperature and pressure, and not on composition of the system. In less concentrated solutions, anions and cations act independently of each other. However, in high concentration solutions like many produced brines, ions are affected by other ions and the chemical behavior of the solution cannot be explained in terms of concentration [1]. Therefore, the equilibrium constant in these more realistic systems are described in terms of species activity. Equilibrium constants need to be expressed in terms of species activity when formation of scale is in question. In other words, the solubility of a complex salt in water is represented with species activities instead of simply concentrations. Equilibrium constant in a non-ideal system (produced brine) can be expressed by:

$$K_{eq} = \frac{\{C\}^c\{D\}^d}{\{A\}^a\{B\}^b} \quad \text{..... (2.4)}$$

Where {C} and {D} are the activity of the species C and D. The solubility of a salt is described as the mass of the salt dissolved in a known mass or volume of a solution. The following general equation is for salts, in which different number of charges of cations and anions are present:

$$M_mX_x(s) \leftrightarrow mM^{z+}(aq) + xX^{z-}(aq) \quad \text{..... (2.5)}$$

In the above equation M is the positively charged element and X is the negatively charged element (e.g. $FeCl_3$, where Fe charge is +3 and Cl charge is -1). Also, m is the number of cations with a charge z^+, and x is the number of the anions with a charge of z^-. In scale formation, the equilibrium constant for dissolution of salts is a crucial parameter of study. For the general dissolution reaction in equation 2.5, the equilibrium constant is:

$$K_{eq} = \frac{\{M^{z+}\}^m\{X^{z-}\}^x}{\{M_mX_x\}} = \{M^{z+}\}^m\{X^{z-}\}^x \quad \text{..... (2.6)}$$

Since the activity of a pure solid is by definition equal to one, $K_{eq}=K_{sp}$, where K_{sp} is the equilibrium constant for the dissolution of a salt, also known as *solubility product* [1]. So Equation 2.6 can be expressed as:

$$K_{sp} = \{M^{z+}\}^m\{X^{z-}\}^x \quad \text{.....(2.7)}$$

The activities of the dissolved ions at equilibrium are a function of temperature, pressure and brine composition. There is a comprehensive compilation of solubility data K_{sp} for various ionic compounds from the CRC Handbook of Chemistry and Physics [2]. These data are important when investigating a potential scaling issue in an oil field. There are many software

and models available in the market to calculate activities of species. Oil field brines usually have a high degree of supersaturation (i.e. the concentration of cations and anions are much higher than predicted by chemical equilibrium calculations). Supersaturated solutions can exist for a long time without any scale formation unless another disturbance in the system takes place, such as a seed crystal or an appropriate surface [1]. An important factor in measuring the potential of a brine solution to form scale is measured by the saturation ratio (SR):

$$SR = \frac{\{M^{z+}\}^m\{X^{z-}\}^x}{K_{sp}} \quad \text{..... (2.8)}$$

Specifically, SR measures the degree of supersaturation. Precipitation can only take place when SR is greater than 1.0. The $\log_{10}$ (SR) is called *saturation index* (S_{ind}). The estimation of S_{ind} is performed by empirical correlations of pH, alkalinity and concentration of dissolved ions and ionic strength of the fluid [1].

The rate at which scale forms is usually described in terms of induction time (t_{ind}), which is the time it takes scale to form after a supersaturation condition exists. In the case that induction time is greater than the residence time of the fluid in supersaturated state in the downhole area (porous media rock and tubulars), the assumption is that scale will not form. Nucleation kinetics theory describes the relationship between induction time and nucleation rate. This theory is characterized by the logarithm of the induction time being proportional to the nuclei surface tension divided by S_{ind} raised to various exponents [1]. An Equation (2.9) based on this theory is shown for the $BaSO_4$ induction time.

Determining scale formation rate is of vital importance and is the first step needed to design and execute a scale prevention plan. In this thesis, barium sulfate ($BaSO_4$) scale is studied specifically. After supersaturation state has occurred and nucleation takes place, it appears that the crystal initially forms as pure barite, and as growth continues, the solution around the crystal has a fewer barium ions than the rest of the solution. Therefore, since the produced water contains other salts, other ions in the solution such as strontium and calcium are most likely to incorporate into the crystal since their relative concentrations become higher. The induction time for barite, in the absence of inhibitor t_{ind}^{0}, can be described by the following equation, which comes from the models of nucleation kinetics developed by Tomson et al. [5]

$$\log(t_{ind}^{0}, sec) = \frac{2.2+[1087-0.3T(K^o)]^2}{T^2 S_{ind}} - \frac{0.12+[1087-0.3T(K^o)]^3}{T^3 {S_{ind}}^2} \quad \text{.....(2.9)}$$

The term in the square brackets is related to the surface tension function from classical nucleation theory. This equation predicts the induction time of the start of scale formation as a function of the saturation index (S_{ind}) and temperature (T). Because solubility of barium in water is a major issue in determining scaling, the above equation is crucial when considering the use of inhibitor to prevent scaling. Furthermore, in the next section, an equation that models the influence of inhibitors on the nucleation or induction time t_{ind}^{inh} will be discussed.

2.4 Scale Inhibition Mechanisms

Inhibitors can be nucleation or crystal growth inhibitors; however all of them act through some combination of both mechanisms. It seems that one or other mechanism predominates for a given chemical. In our case, SI, the commercial scale inhibitor used, is predominantly a crystal growth inhibitor.

2.4.1 Nucleation Inhibition

Scale inhibition is measured by static and dynamic efficiency and adsorption tests that will be discussed in Chapter 3. Based on experimental data, even though the sulfonate chemicals are less effective at preventing barite nucleation, the low efficiency at the beginning is followed by a prolonged low concentration and accompanied by an increase in inhibition efficiency [3]. Once nuclei have formed, they are prevented from growing any further and the inhibitor which remains in solution effectively suppresses nucleation at the new, lower supersaturation. It is believed that these sulfonate molecules are absorbed at the active growth sites on the barite surfaces [5].

2.4.2 Crystal Growth Inhibition – Adsorption

There are several types of inorganic mineral scale and scientists have developed chemicals (functional groups) specifically for inhibiting certain minerals. The inhibitor molecule should not precipitate with the scale-forming ions, but, at the same time, should have affinity for the lattice ions [8]. The commercial scale inhibitor used in this thesis consists of carboxylic

acids with sulfonate substitutions. This type of chemical is designed to inhibit barium sulfate scale by an adsorption mechanism explained in detail by Burton, Cabrera and Frank (BCF).

One of the most common and most studied precipitation kinetics theories is BCF spiral growth mechanism. As explained in Section 2.2, kink sites grow continuously in a spiral, thus overcoming the expected activation energy for nucleation and creating new potential scale-forming sites. An important part of this theory is that inhibition of scale is believed to occur due to the absorption onto the scale-friendly surface of a blocking agent that stops spiral growth. Only the active growth sites needs to be in contact with the scale inhibitor to prevent the advance of the spiral. In order to study inhibitor effectiveness in terms of molecular parameters that can be measured, adsorption isotherms, the minimum inhibitor concentration (MIC) and the induction time in the presence of inhibitor concentration t_{ind}^{inh} must be determined. Therefore, a comprehensive study of the kinetic and thermodynamic aspects of adsorption and nucleation is crucial in order to achieve the objective of this thesis.

The ultimate concern is to tackle an important issue affecting flow assurance, which is to find a minimum inhibitor concentration (MIC). This will be achieved by the determination of adsorption of the inhibitor molecules onto sand, and induction time in the presence of inhibitor concentration. The overall goal of the inhibitor treatment is to provide the longest protection time possible before another intervention is required. The experimental determination of scale inhibitor adsorption is described in Chapter 3.

Tomson et al. [5] proposed that the primary driving force for adsorption is related to simple hydrophobic repulsion from solution of a macroneutral molecule. In addition, based on nucleation studies, it was observed that the inhibitor concentration needed to effectively inhibit

barite formation is approximately equal to 16% surface coverage of the active growth sites. An equation that describes induction time for barite in the presence of inhibitor is an important parameter to predict the minimum inhibitor needed:

$$Log_{10}\left(t_{ind}^{inh}, sec\right) = Log_{10}(t_{ind}^{0}, sec) + b_{inh}\left(\frac{L}{mg}\right) * C_{inh}\left(\frac{mg}{L}\right) \quad \text{.....(2.10)}$$

Where, C_{inh} is the concentration of inhibitor added and b_{inh} is an inhibitor effectiveness term. According to Tomson et al. [5] this equation works well for a large range of inhibitors and minerals, but is not mechanistic in origin. In addition, the empirical term b_{inh} is a function of temperature, pH, and pressure differences. The advantage of this equation for modeling the effect of inhibitors is that the basic nucleation phenomenon is modeled separately from the scale forming mineral inhibition effect. However, there is no exact fundamental understanding of b_{inh} and a comprehensive investigation of inhibitor effectiveness for a new inhibitor or for different conditions is needed.

In addition, Graham and Mackay [7] addressed another mechanistic explanation of inhibition of barium sulfate. They proposed that the inhibition arises from adsorption of a Ca-phosphonate complex from solution onto specific sites on the developing crystal [7]. Figure 2.3 illustrates this inhibition mechanism. Furthermore, this study concluded that 10 to 25% coverage of the critical sites causes nearly 100% of inhibition of scale formation. This agrees with Tomson et. al.'s results [5]. According to Graham and Mackay [7], an inhibitor concentration greater than the MIC causes the Ba^{2+} ions to stay in solution and greatly reduces the amount of scale on the

surface. Concentrations greater than the MIC actually increase adherence of the scale and change the crystal structure in a disadvantageous manner.

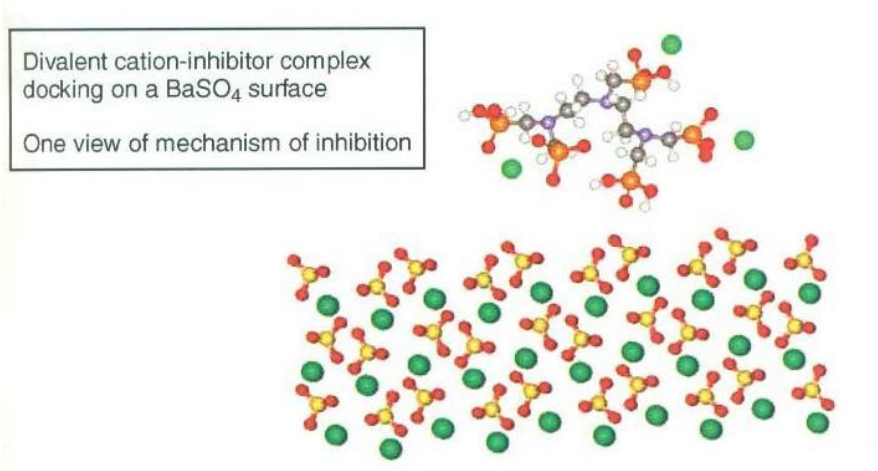

Figure 2. 4 Generalized inhibition mechanism by Graham et al. 2004

In addition, there have been studies of synthesized Polyvinyl Sulfonate (PVS) that suggest that molecular weight plays a role in the mechanism of adsorption. In other words, these studies found that adsorption increases with molecular weight (Mw) of the polymer [10]. From an inhibition viewpoint, intermediate-Mw material is more effective at preventing nucleation of crystals, but higher-Mw polymers inhibit crystal growth better than lower-Mw polymers.

2.4.2.1 Adsorption of scale inhibitor on barium sulfate

The strong connection between adsorption and inhibition becomes even clearer with an study by Breen et al. [9]. A series of phosphonates were synthesized and their inhibition efficiency was measured at pH 4 and 85^{o}C using both seeded and unseeded static efficiency tests. The adsorption enthalpy (ΔH_{ads}) and entropy (ΔG_{ads}) were calculated using equations reported by

Naono [10] . In both cases, adsorption was found to be endothermic, with ΔH_{ads} in the range 2060 -13142 $J \cdot mol^{-1}$. These studies showed that adsorption was driven by a favorable entropy change, with ΔS_{ads} in the range 62.7 – 103.8 $J \cdot mol^{-1} \cdot K^{-1}$, therefore, the overall free energy given by the well-known expression in Equation 2.11 was negative.

$$\Delta G = \Delta H - T\Delta S \quad \text{..... (2.11)}$$

The increase in entropy on adsorption is believed to be caused by the release of water molecules which had previously been bound to the inhibitor molecules [3]. Inhibitors with standard entropies of adsorption less than 42 $J \cdot mol^{-1} \cdot K^{-1}$gave poor results in the static efficiency tests. Therefore, the authors suggested that good inhibitors should have minimal hydrophobic content. Also, they hypothesized that adsorption blocking active growth sites at the crystal surface was the principal inhibition mechanism in the seeded tests.

2.4.2.2. Scale Inhibitor Adsorption onto Quartz

The adsorption of scale inhibitor on silica is of crucial importance for squeeze treatments, and this is the main subject of this thesis. The surface charge of a mineral is governed by the concentration of its ions in the surrounding medium, and is therefore dependant on pH [25]. Consequently, adsorption of material on the mineral is influenced by the surface charge. Based on previous work by Laing [3], adsorption of phosphonate type inhibitors decreases as the pH increases from 2 to 6. Increasing pH reduces adsorption because of the electrostatic repulsion between the surface and the inhibitor i.e. both the inhibitor and the quartz surface charge become

more negatively charged. According to Laing [3], when calcium ions are present, they adsorb strongly on the quartz surface at pH values greater than four, increasing the surface charge to the neutral range. Therefore, this results in an observed increase in inhibitor adsorption. Thus, based on experimental observations, this adsorption mechanism at pH values greater than four is by electrostatic bridging through calcium ions and not by hydrogen bonding . However, at lower pH values, the fact that the greatest adsorption occurs at pH values where the inhibitor is protonated (which might be due to calcium complexation) suggested the predominant mode of adsorption is hydrogen bonding to negative sites on the silica surface [3].

In another study by Laing [3], the influence of calcium on inhibitor adsorption was significant. He measured the commercial inhibitor DETPMP (Diethylenetriamine penta methylenephosphonic acid) adsorption at pH 2, 4 and 6 in both 428 ppm synthetic calcium-containing sea water and a calcium free synthetic seawater. The major difference was at pH 6, when adsorption was approximately six times higher with than without calcium. Also, calcium concentration was found to be considerably lower than those at pH 2 and 4 for the same inhibitor concentration. This confirms the theory that calcium ions which adsorb into silica, result in a positive influence on inhibitor adsorption. The results of this study are shown in Table 2.1. Γ_{max} represents the adsorption of scale inhibitor per mass. And the values in brackets are the calcium concentration in parts per million (ppm).

Table 2. 1 DETPMP Adsorption Results on Silica (Laing, 2006)

DETMP Adsorption on Crushed Silica Core With and Without Ca^{2+} Ions			
pH	Γ_{max} / mg ·g^{-1} $[Ca^{2+}]_{initial}$ = 0 ppm	Γ_{max} / mg ·g^{-1} $[Ca^{2+}]_{initial}$ = 415 ppm	**$[Ca2+]_{final}$/ppm**
2	1.4	1.7	460
4	0.5	0.7	445
6	0.2	1.5	375

In summary, according to the literature, adsorption of scale inhibitor on sandstone rock decreases with increasing pH due to silica's surface negative charge increment as a function of pH, thus, creating an electrostatic repulsion between the already negatively charged silica and the scale inhibitor. Also, adsorption is positively affected with a higher inhibitor molecular weight and calcium ions yield a better adsorption due to their neutralization properties on the rock surface charge. In other words, adsorption is definitely influenced by surface charge. Therefore, the major mechanism of scale inhibitor adsorption on silica is electro-adsorption, which is driven by coulombic forces, and is strongly pH dependant as a result.

Chapter 3

Experimental Materials, Equipment and Procedures

The materials, equipment and procedures used in the experimental study of the scale inhibitor (SI) are presented in this chapter. Section 3.1 describes the materials used, including the synthetic brine solutions, the scale inhibitor solutions and the materials used to construct the porous media. Section 3.2 reviews the experimental apparatus constructed to conduct the displacement experiments. Section 3.3 describes the overall equipment used in this study. Finally, Section 3.4 explains the procedures followed in the study, including the preparation of the solutions, the injection through porous media and the analytical testing of effluent and injected solutions.

3.1 Materials

This research was conducted to determine the adsorption of scale inhibitor SI on silica sand contained in sandpacks. The chemical was obtained from ConocoPhillips and its properties are described in Section 3.1.1. Preparation of the SI solutions is discussed in Section 3.1.2. The scale inhibitor was diluted in two fluids to study adsorption on silica sand. First, it was diluted in reverse osmosis (RO) water and second, mixed with synthetic seawater (SW) of composition provided by ConocoPhillips. A synthetic field brine (FB) was used to displace the scale inhibitor solution from the sandpacks. Both SW and FB compositions are described in Section 3.1.3. Sandpacks are described in section 3.3.3.

3.1.1. Scale Inhibitor

A commercial scale inhibitor provided by ConocoPhillips is composed of approximately 30 % polyvinyl sulfonate (PVS). Figure 3.1 shows a schematic structure of PVS. According to the MSDS (Material Safety & Data Sheet, the remaining components include carboxylic acids. There is also free sulfate.

Analysis of effluent samples for SI was based on measurement of sulfur using Inductively Couple Plasma Atomic Emission Spectrometry (ICP-AES). Since the commercial SI solution contains sulfate, it was necessary to remove the sulfate by dialysis. The commercial SI sample contained 3.28 wt% of sulfur. Preparation of SI samples is described in Section 3.3.7. The density of the sample was 1.24 g/cm^3 at room temperature (25 ^{o}C).

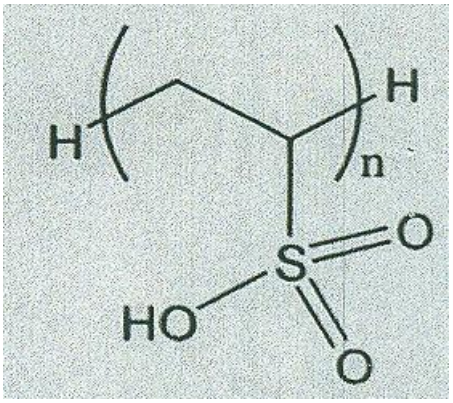

Figure 3. 1 Polyvinyl Sulfonate (PVS) chemical structure (Laing, 2006)

3.1.2 Scale Inhibitor Solution Preparation

The scale inhibitor solution was received from ConocoPhillips in a 1.5 gallon bottle. The MSDS states that the solution consists of polycarboxylic acids in water. The composition of each constituent was not known. As noted earlier, 30% of the scale inhibitor consists of PVS.

In field applications, 5 wt% of the stock chemical is mixed with SW and injected through a squeeze treatment. Therefore, the experiments were conducted with scale inhibitor concentration of 5 wt % in SW and RO water. The details of each experiment are discussed in Section 3.4.6.

3.1.3 Synthetic Seawater and Field Brine Compositions

The SW compositions used in these experiments are presented in Table 3.1 and the composition of synthetic field brine is presented in Table 3.2. The densities of SW and FB are 0.98 and 0.92 g/cm^{3}respectively at 25 °C.

Table 3. 1 SW composition provided by ConocoPhillips

Salt	Molecular Formula	Weight Percentage	ppm
Sodium Chloride	NaCl	2.3499	23,499
Potassium Chloride	KCl	0.0725	725
Calcium Chloride	$CaCl_2{\cdot}2{\cdot}H_2O$	0.1467	1,467
Magnesium Chloride	$MgCl_2{\cdot}6H_2O$	1.0625	10,625
Sodium Sulfate	Na_2SO_4	0.392	3,920

Table 3. 2 Field brine composition provided by ConocoPhillips

Salt	Molecular Formula	Weight Percentage	ppm
Sodium Chloride	NaCl	2.479	24,790
Potassium Chloride	KCl	0.0382	382
Calcium Chloride	$CaCl_2 \cdot 2H_2O$	0.055	550
Magnesium Chloride	$MgCl_2 \cdot 6H_2O$	0.0837	837
Barium Chloride	$BaCl_2 \cdot 2H_2O$	0.0107	107
Strontium Chloride	$SrCl_2 \cdot 6H_2O$	0.0046	46

3.1.4 Silica Sand

Ottawa F-110 Silica from U.S. Silica Company (Berkeley Springs, WV) was used to make the 1.5 inch × 1 foot long sand packs. The sand grain size distribution is shown in Table 3.3.

Table 3. 3 Size distribution for Ottawa sand as percent retained on sieve

USA Sieve Size	40	50	70	100	140	200	270	Pan
% Retained	0	1	4	19	41	25	8	2

3.2 Displacement Experimental Apparatus

The displacement apparatus was designed and built to inject and displace scale inhibitor solutions into the sand packs, measure the pressure drop across the porous media during the experiments and collect effluent samples for analysis. The equipment consist of a pump, transfer cylinders, sand pack holder, pressure transducers, fraction collector, and all the necessary tubing and valving to complete the setup. The sandpack was partially surrounded with a stainless steel

semi cylinder to control the temperature of the sandpack. Heat was provided by a 100 W electrical heater. Displacement experiments tests were conducted at 70°C. A computer operated switching valve was acquired for some of the experiments to obtain a more accurate change of fluids during the displacement experiments. A diagram of the original setup is shown in Figure 3.1. Figure 3.2 describes the updated setup with the new switch valve and the temperature control system

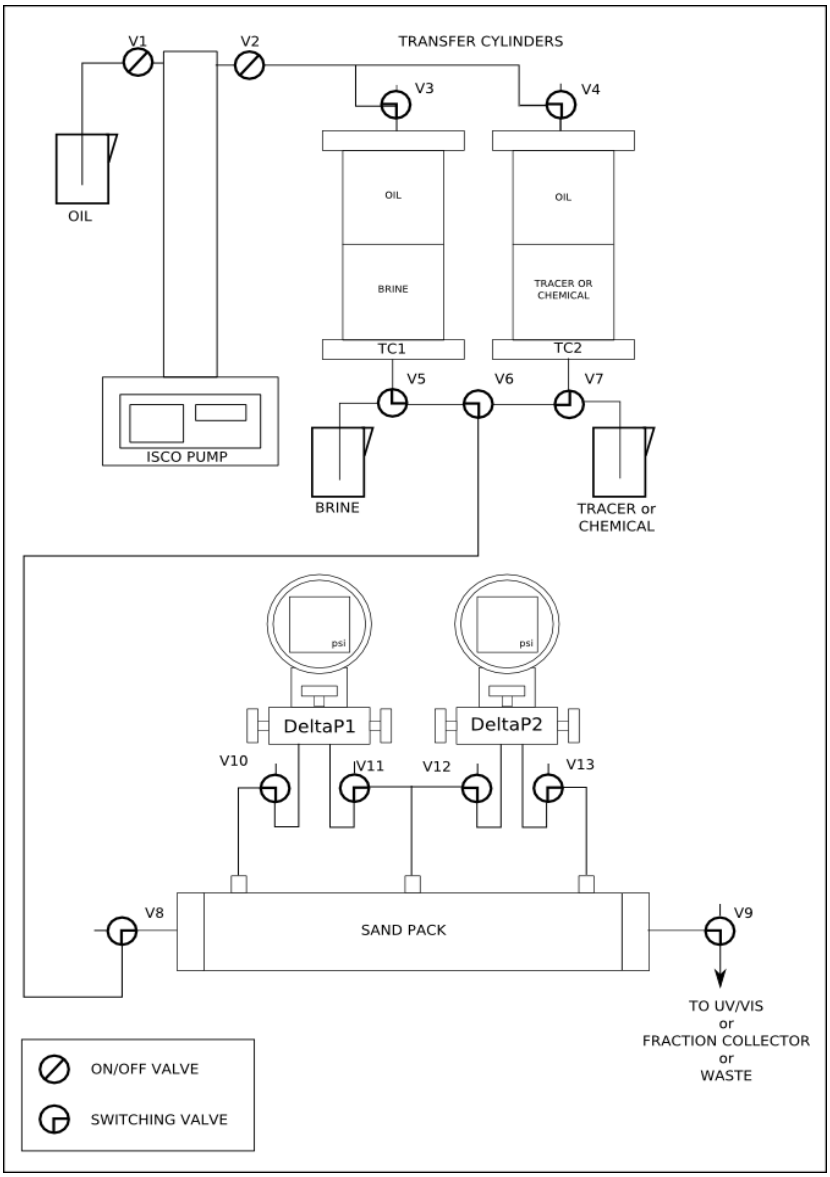

Figure 3. 2 Diagram of original setup (Courtesy of Stephen Johnson)

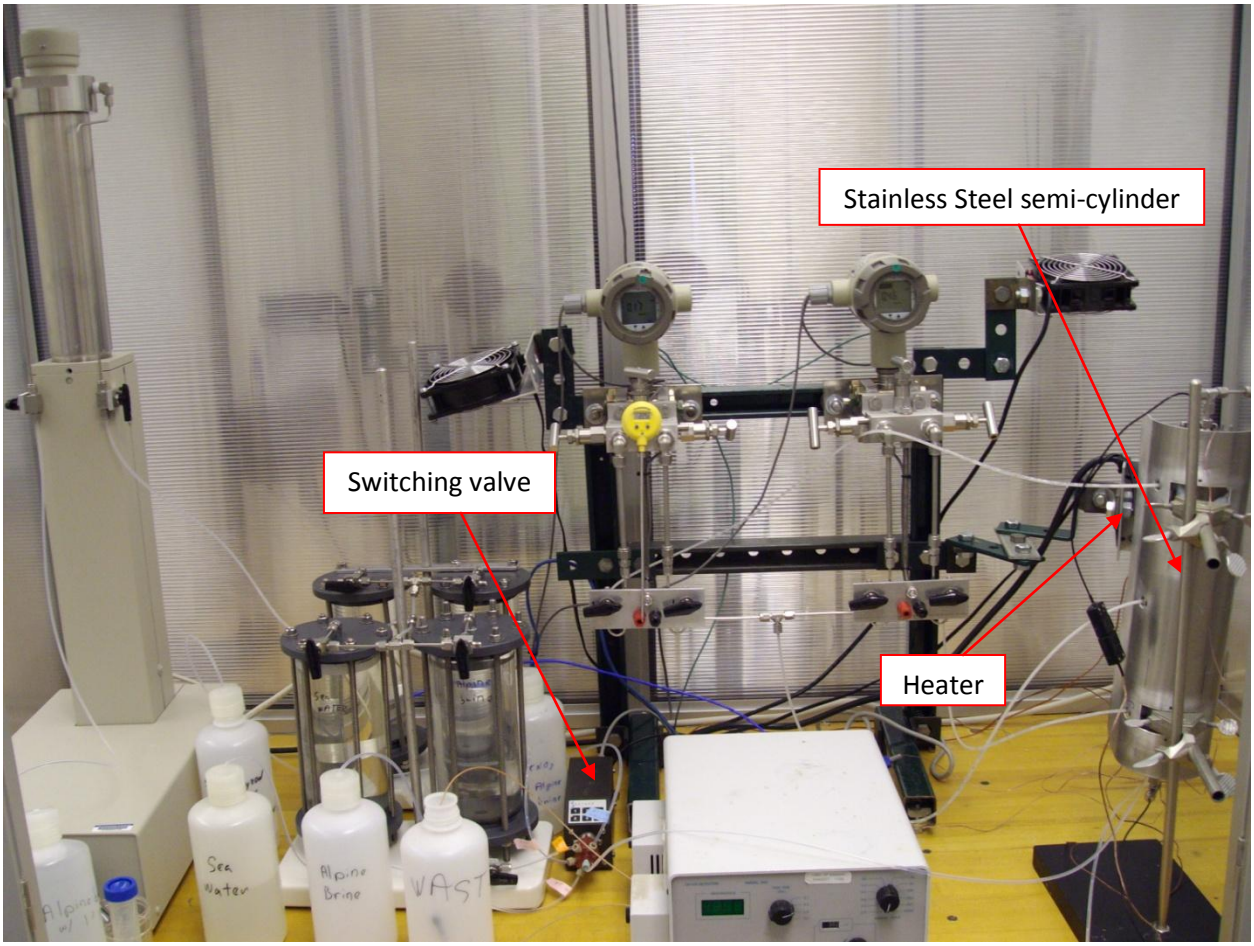

Figure 3. 3 Picture of the latest setup used showing the new equipment

In both setups, a syringe pump displaced Soltrol 130 (Chevron Phillips Chemicals Co., The Woodlands, TX) into the transfer cylinder containing the brine, tracer or scale inhibitor solution. From the transfer cylinder, the solution flowed though a 1/8 inch OD fluorinated ethylene propylene (FEP) tubing to the sand pack. Honeywell differential pressure transducers were connected to three pressure ports to measure the pressure drop across the sand pack in two sections. Data from the pressure transducers, the pump rate and Abs_{290} were recorded by the data

acquisition program Labview. Effluent exiting the sand pack holder flowed through the absorbance spectrometer and was collected with a fraction collector in samples of 0.1 pore volume.

Effluent samples were analyzed to determine ultra violet light absorbance at 290 nm, a set of elemental concentrations (sulfur, barium, strontium, calcium, magnesium and silicon), pH and particle size. A Perkin Elmer Lambda 20 UV/Vis spectrometer was used to determine absorbance, the ICP-AES, model Optima 2000 D.V. manufactured by Perkin Elmer Inc. was used to determine concentrations, a portable Horiba pH meter yielded pH values and the particle size of the samples were found by using a Brookhaven Zeta PALS particle size analyzer (Holtsville, NY). These tests are described in more detail in Section 3.4.

3.3 Experimental Equipment

In this section, the equipment used in the experimental setups and the analytical testing of the scale inhibitor adsorption are described in additional detail.

3.3.1 Pump

The pump used in order to inject fluids through the sand pack was a 1 liter capacity syringe pump manufactured by Teledyne Isco Inc. (Lincoln, NE), model 1000D. This type of pump was designed to handle high pressure, high viscosity liquids and its injection rate ranges from 0.1 to 400 ml/min with a precision of 2.5 % full scale with regards to the flow rate. This piston-driven pump, which uses a single speed gear train, is connected to a programmable multi-pump controller interface that is compatible with the data acquisition system Labview. This pump was used to inject the scale inhibitor material and perform permeability and tracer tests.

3.3.2 Sand Pack holder

The sand pack holder was fabricated from poly-ethyl-ethyl-ketone (PEEK), which exhibits excellent resistance and dimensional stability to high temperatures and harsh environment (reservoir conditions). This material is chemically resistant and insoluble in common solvents including acids, salts and oil. It features low outgassing, low particle generation and inherent purity for reduced contamination. The sand pack inside diameter (ID) was nominally 1.35 inches and the outside diameter (OD) was 1.75 inches. Its length was 12 inches. Two nylon screens were used at either end of the sand pack to retain sand. The screen in contact with the sand has a mesh size of 330 and the screen in contact with the end cap has a mesh size of 37. End caps of 1.75 inches OD were installed using eight screws and sealed with o-rings. A schematic of the end cap and the sand pack holder is shown in figure 3.2.

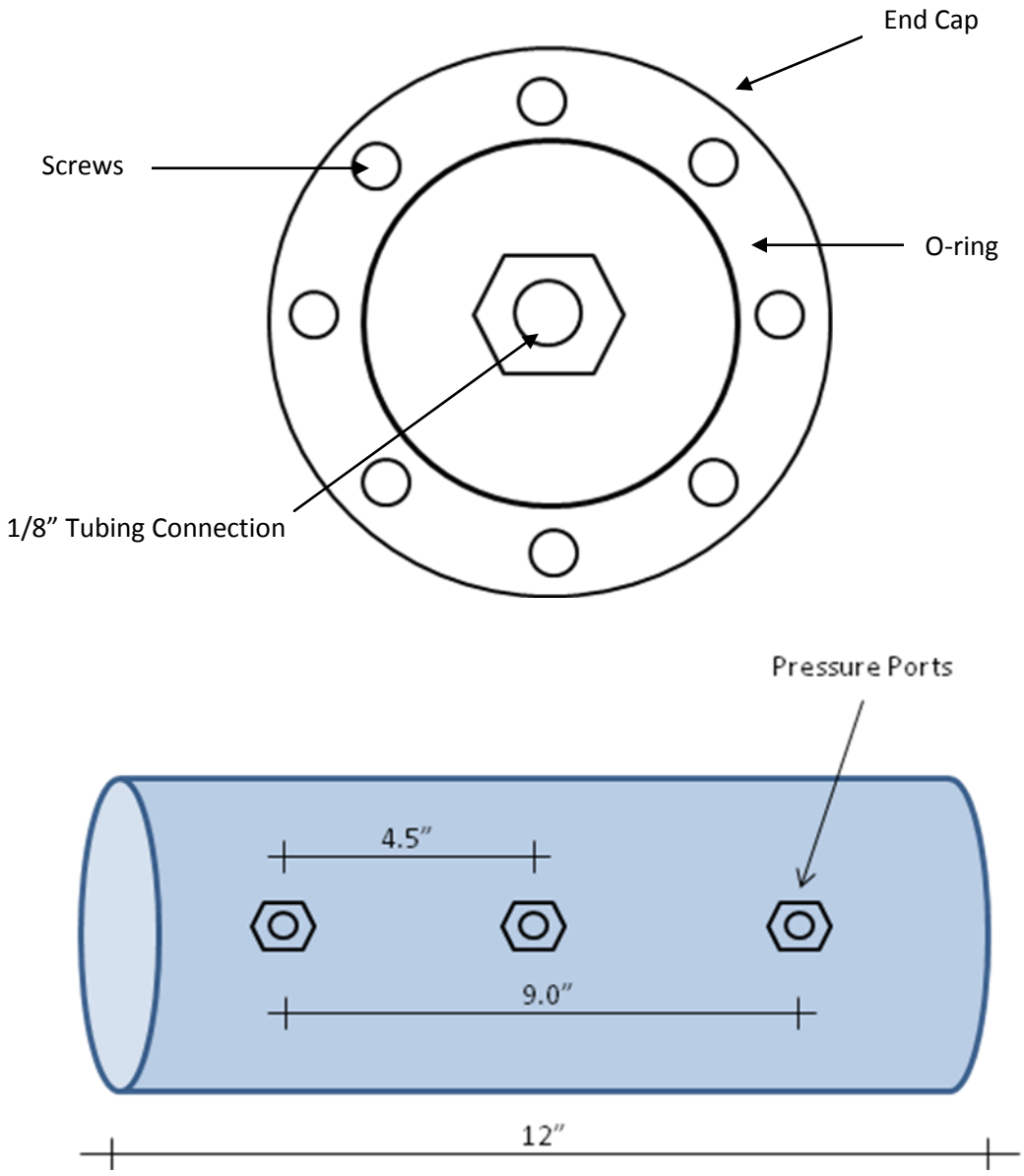

Figure 3. 4 Sand pack holder and end cap design

The sand pack holder had 3 pressure ports evenly spaced in order to measure pressure differential during injections. The ports were centered 4.5 inches apart and the total distance between the first and the last pressure port in the sand pack holder was 9 inches. Pressure was measured across two sections, Section 1 and Section 2, each 4.5 inches in length. Also, each

pressure port has a PEEK fitting that screwed into the port and a 215 mesh nylon screen was placed at the sand/fitting interface to ensure no solids could escape into the transducer lines.

3.3.3 Sand Packs

Four sand packs were used in the experimentation of scale inhibitor solutions injection. Each sand pack was made with the sand pack holders described in Section 3.2.2 and the silica sand described in Section 3.2.1. The physical characteristics of each sand pack are shown in Table 3.4

Table 3. 4 Sand packs physical characteristics

Sand Pack	Pore Volume (ml)	Porosity	Permeability (D)
PEEK #1 04/19/10	101.7	0.351	4.01
PEEK#1 05/18/10	100.1	0.347	4.08
PEEK#2 05/24/10	103.2	0.364	4.22
PEEK#1 05/25/10	102.1	0.358	4.13

PEEK #1 04-19-10	
Section	**Permeability (D)**
1	3.94
2	4.08
Overall	4.01

PEEK #1 05-18-10	
Section	**Permeability (D)**
1	4.03
2	4.13
Overall	4.08

PEEK #2 05-24-10	
Section	**Permeability (D)**
1	4.16
2	4.28
Overall	4.22

PEEK #1 05-25-10	
Section	**Permeability (D)**
1	4.11
2	4.15
Overall	4.13

3.3.4 Ultraviolet/Visible Spectrophotometer

The in-line UV/Vis detector was a ProStar Model 340 manufactured by Varian Inc. (Palo Alto, CA), and was used during tracer tests and scale inhibitor injection in each sand pack. The detector measures the absorbance of light in a range of wavelengths from 190 to 800 nm. A deuterium lamp is used for the wavelengths between 190 and 360 nm. The tracer used was 0.1 M potassium nitrate (KNO_3) which was detected at 302 nm. The off-line UV/Vis detector, model Lambda 5 manufactured by Perkin Elmer Inc. was used to measure absorbance at 290 nm of the collected scale inhibitor solution samples.

3.3.5 Pressure Transducers

Honeywell differential pressure transducers (Model ST 3000) were used to measure the pressure differential across the sand packs during porous media displacement experiments. The accuracy of these transducers is claimed by the manufacturer to be 0.2 % full scale.

The output of each transducer is an AC voltage, so when using the Labview data acquisition system, which only reads a DC voltage, a demodulator box was installed to convert the AC reading from the transducer into a DC reading that was compatible with Labview.

3.3.6 Fraction Collector

An ISCO Retriever IV Fraction Collector was used during the displacement experiments. It can be manually programmed to collect samples on a basis of time, counted drops or electronic pulses from a peristaltic pump. The tube capacity for the collector is 190, 17 ml vials or 133, 25 ml vials. The sample collecting was conducted in 25 ml vials and time was the basis to control the effluent volume of each vial; thus, it was easier to keep track of material balance since injection rate was constant.

3.3.7 Inductively-Coupled Plasma Atomic Emission Spectrometry (ICP-AES)

ICP model Optima 2000 DV manufactured by Perkin Elmer Inc. was used to determine the amount of certain elements in given aqueous sample by making these elements emit a characteristic wavelength specific light that can be measured. The ICP hardware is designed to generate plasma (gas in which atoms are present in an ionized state) which is then maintained by inductive heating of the flowing carrier gas into the ICP torch. The purpose of this gas, which is usually argon or nitrogen, is to convey the sample to the plasma. Once the nebulizer transforms the aqueous solution sample into an aerosol it is carried into the plasma torch and the light emitted by the atoms of an element in the ICP is detected and converted to an electrical signal that can be measured quantitatively. The intensity of the signal is compared to previous measured intensities of known concentrations of the element and a concentration is computed. The samples that were collected from the porous media displacement experiments were diluted according to the element of choice for which the samples needed to be tested. For example, in order to test for barium concentration, the samples were diluted 10 times, and to test for sulfur concentration they were diluted 100 times. The elements measured were sulfur, calcium, magnesium, barium, strontium and silicon. The uncertainty in determining these elements' concentration was +/- 10%.

3.4 Experimental Procedures

This section describes detailed experimental procedures used during the study. These include the preparation and characterization of sand packs, synthetic brines and scale inhibitor solutions, displacement procedures, and the analytical testing of samples.

3.4.1 Sand Preparation

The sand that was used in the making of the sand packs (Section 3.3.3), was Ottawa F-110 sand. The sand was sieved, acid washed and dried before use. The sieving of the F-110 sand was done to discard all +50 mesh material. This was accomplished by passing approximately 5 kg of sand through a 50 mesh sieve to remove large grains. After that, the sand was acid washed to remove soluble metals, including iron, manganese, aluminum, and other.

The acid washing was done by placing the sieved sand into a 2.5 L acid bottle with 1 M HCl under a fume hood. The acid was poured into the bottle first and then the sand was slowly added using a funnel until it reached the top of the acid. The bottle was then sealed and shaken to ensure each sand grain was in contact with the acid. After that, the sand submerged into the acid was allowed to soak for at least 24 hours and then the extra acid was poured off and the sand was rinsed with approximately 10 liters of RO water.

The wet sand was then poured off into a Buchner funnel connected to the water aspirator and the water was aspirated out for at least five minutes. Then the water aspirator was stopped and the Buchner funnel filled again with RO water to rinse the sand further. As soon as the aspirator was started again the sand was agitated by hand while the water was evacuated from the filtered funnel so that the less dense organics present in the sand migrated towards the center. These organics were then removed with a plastic spoon from the center of the dried sand, and this washing process was repeated several more times with large amounts of RO water, until the acid was completely washed and negligible organics were left. The washed sand was placed in an aluminum pan and dried in the oven at 75 °C for at least 24 hours.

3.4.2 Sand Packing

Sand packs were constructed by installing all fittings and pressure testing for leaks. The PEEK pressure port fittings were wrapped with high temperature silicone sealant which is effective up to 150 °C. The end caps were sealed with screws and o-rings. A three way stainless steel valve was connected to the inlet end cap and a pressure gauge and a two way valve was connected to the outlet. Once the pressure ports fittings were into place and the end caps were installed, the sand pack holder was pressurized to 90 psi with air. The valves were closed and pressure was monitored using the gauge over several days to ensure that no air left the sand pack through any possible leaks.

After the pressure testing was passed, the sand pack was filled with sand. The first step was to determine the sand density. This was achieved by weighing the amount of sand needed to fill a 100 ml graduated cylinder under vibration. Since mass = density × volume, the bulk volume of the sand pack holder is known and by multiplying it by the density, we have an idea of how much compacted sand should fit into the sand pack holder under vibration.

The outlet end cap was sealed with a plastic temporary flat cap to ensure that sand was retained during vibration. Then the sand was poured using a funnel through the inlet of the sand pack. At the same time, a Syntron Magnetic Vibrator, model V-4-AC manufactured by FMC Technologies (Houston, TX) was applied to the outside wall of the sand pack to ensure optimal compact packing. When the all the sand entered the sand pack, the funnel was removed and the 330 mesh nylon screen was placed in contact with the sand, immediately after, the 37 mesh screen was placed on the sand pack and finally the end cap was put on with the o-ring seal the screws. The holder was inverted and the process was repeated. The end cap was installed again

with the filters and the sand pack was ready for another pressure test. Once the filled-sand pack pressure test passed, the sand pack was ready for characterization.

The weight of the sand-filled sand pack was measured. Then, it was connected to a gear pump, model number 7144-00, (March MFG, Inc, Glenview, IL). The purpose of this pump was to inject high quantities of RO water at high injection rate through the sand pack to settle the sand, displace the air that could affect the compressibility and eliminate small sand particles before any displacement test. Once several gallons of RO water were injected, the valves were closed and the now fully saturated sand pack was weighed. The reason for this procedure was to calculate porosity, using equations 3.1 - 3.3.

$$Porosity = \frac{Pore\ Volume}{Bulk\ Volume} \quad \text{..... (3.1)}$$

Where,

$$Pore\ Volume = \frac{Wet\ Weight - Dry\ Weight}{R.O.Water\ Density} \quad \text{.....(3.2)}$$

And,

$$Bulk\ Volume = \pi r^2 h \quad \text{.....(3.3)}$$

Where,

r = Inner sand pack radius (cm)

h= Sand Pack length (cm)

3.4.3 Permeability Calculation

The permeability was determined by injecting field brine (Section 3.1.2) at flow rates of 5, 10 and 20 ml/min as pressure data was acquired. Each rate was maintained long enough to reach a steady state pressure drop. Permeability was calculated from Darcy's Law, equation 3.4.

$$k = \frac{Q \ \mu \ L}{A \ \Delta P} \quad \text{..... (3.4)}$$

Where,

k = Permeability, Darcy

Q = Flow Rate, ml/s

μ = Viscosity, cp

L = Length, cm

A = Cross sectional area, cm^2

ΔP = Pressure drop, atm

3.4.4 Tracer Test

The objectives of the tracer tests were to evaluate the homogeneity and quality of the sand pack and to verify pore volume. An in-line UV/Vis detector was used to measure the absorbance of the tracer solution from the effluent of the sand pack. The tracer was 0.1 M KNO_3 in field brine, which was detected at a wavelength of 302 nm. The deuterium lamp in the UV/Vis detector needs approximately 30 minutes to warm up. Once this occurred, the detector was zeroed at the beginning of the tracer test while injecting field brine without KNO_3 at 5 ml/min.

Data collected from the UV/Vis detector was used to calculate the pore volume and to verify the uniformity of the sand pack. The absorbance was normalized and plotted versus the volume injected into the sand pack; then the area under and above the curve was calculated via the trapezoidal rule. The pore volume was simply the amount of fluid injected at which the two areas were equal. The characteristic shape of the absorbance curve was used to graphically verify the homogeneity of the sand pack. This curve had to have an S shape and rise quickly from zero to the injected concentration of KNO_3 without having a lead in or tail. If the curve did not present these characteristics then the sand pack either had channels or air trapped. Therefore, the sand packing procedure needed to be repeated since a homogenous sand pack was required for scale inhibitor tests.

3.4.5 Scale Inhibitor Dialysis

The scale inhibitor is known to contain 30% PVS, carboxylic acids and sulfate. ICP analysis on sulfur concentration showed that SI contains 3.28 wt% of sulfur. The ICP (Section 3.3.7) is designed to measure concentrations of pure elements. ICP will detect any sulfur derivative such as sulfate and sulfonate. Therefore, it was necessary to remove the sulfate from the scale inhibitor to study adsorption of SI.

Dialysis is a diffusion process in which can be used to separate solutions containing constituents which have significantly different molecular weights and corresponding size in solution. In dialysis, transfer of molecules through a selectively-permeable membrane is driven by a concentration gradient. In this experimental program, sulfate was dialyzed from the SI solution using a selectively-permeable nitro cellulose 2KDa MWCO membrane (Slide-A-Lyzer ® Dialysis Cassette; model 66230 manufactured by Pierce Inc., Rockford, IL). In theory, any element, molecule, ion or particle with a molecular mass of less than or equal to 2000 daltons such as sulfate passed through the membrane while the PVS will remained in the original solution.

The scale inhibitor sample was inserted into a hermetically closed dialysis cell which was placed into an RO water-filled 5-gallon bucket with a magnetic stirrer in the bottom. As the water flows outside the membrane, the smaller solutes or molecules (sulfate) inside the membrane pass through it leaving the cassette. The membrane blocks the passage of larger substances such as polymers. Figure 3.5 shows the empty cassette, then filled with 20 ml of SI and after 2 to 3 days of dialysis, filled with RO water and substantially sulfate free SI. A material balance was not done on the sulfate.

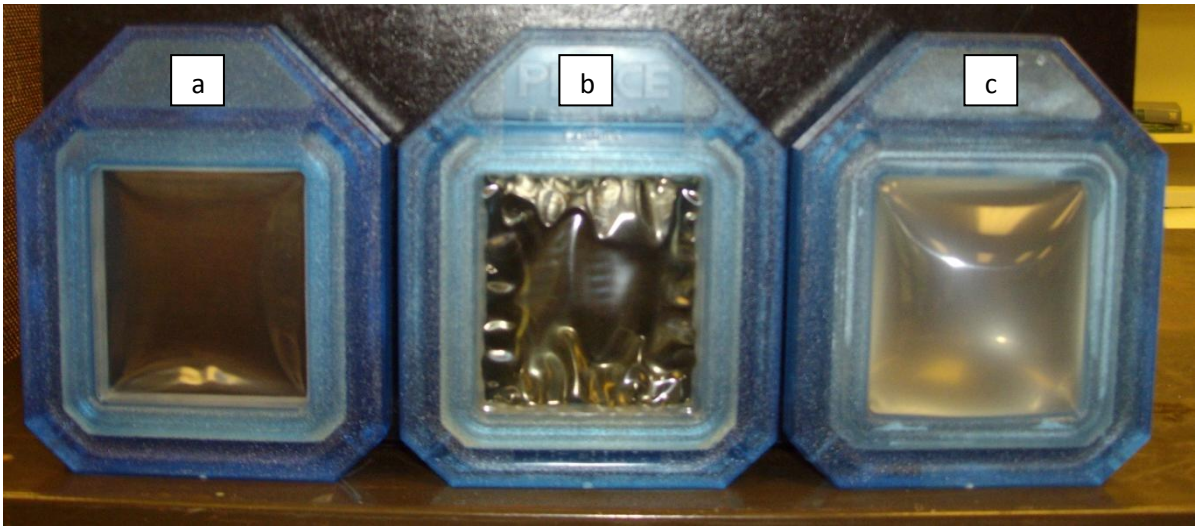

Figure 3. 5 Dialysis cassette empty (a), loaded with SI (b), and after dialysis (c)

3.4.6 Adsorption Tests

The objective of this thesis is to study the adsorption of the scale inhibitor on silica sand.

3.4.6.1 Displacement Experiments

Four displacement tests were conducted to study: 1) the behavior of scale inhibitor in contact with field brine, 2) the interaction of scale inhibitor mixed with SW in the presence of field brine, 3) the mixing between SW(containing sulfate) and field brine(containing barium) and 4) the displacement of 5% SI in RO by RO water. All displacement tests were performed at 70 °C and are named experiment 1, 2, 3 and 4 respectively. Table 3.5 shows the solutions used in each experiment. In each experiment, 3PV of solution containing SI were injected and the sandpack was shut in for 24 hours. Then the resident solution was displaced by the displacing solution indicated in Table 3.5

Table 3.5 Conditions for SI adsorption experiments

Experiment #	Sand pack Name	Initial Saturating Fluid	Injected Fluid	Displacing Fluid
1	PEEK #1 04/19/10	Field Brine	5 % dialyzed SI in RO water	Field Brine
2	PEEK #1 05/18/10	Field Brine	5 % dialyzed SI in SW	Field Brine
3	PEEK #2 05/24/10	Field Brine	Synthetic Seawater (SW)	Field Brine
4	PEEK #1 05/25/10	RO Water	5 % dialyzed SI in RO water	RO Water

3.4.6.1.1 Experiment 1 – 5 % Dialyzed SI in RO Water Injection

The sandpack was initially saturated with field brine. Immediately after, the heater was turned on, field brine was injected at 3 ml/min until a steady pressure drop was observed. The data collection, including pressure drop, flow rate, absorbance and temperature, also started at this point. It takes approximately 40 minutes for the porous media system to reach 70^{o}C; once the thermocouple, which was installed in the three-way-valve at the end of the sand pack to measure the effluent temperature, showed that temperature has achieved steady state, the valves were switched from field brine to the injection of 5% of SI in RO water and sample collection of 0.1 pore volume (PV) vials (about 10 ml) began.

Three pore volumes of 5% dialyzed SI in RO water were injected. After that, the sandpack was shut in for 24 h. Injection was resumed with field brine at 1.48 ml/min (20 ft/day). The sampling collection time step was adjusted for the new injection rate to match the same sampling volume of 0.1 PV.

The rapid injection of scale inhibitor displacing field brine compared to the slower injection of field brine displacing scale inhibitor was done to simulate a squeeze job under reservoir conditions. Approximately 50 PV of field brine was injected at 1.48 ml/min. Analysis of selected effluent samples indicated that changes in fluid compositions occurred in the first 5 pore volumes or approximately 50 vials. Therefore, after the experiment was concluded, these

samples are tested for off-line absorbance, pH and particle size before concentration analysis by the ICP. Sulfur concentration is determined by the ICP and scale inhibitor adsorption was calculated by material balance on the effluent samples.

3.4.6.1.2 Experiment 2 – 5 % Dialyzed SI in SW Injection

The displacement experiment procedure from Experiment 1 (Section 3.4.6.1.1) was followed, except that 5% of the dialyzed scale inhibitor solution was mixed with SW instead of RO water. The reason for isolating SW from the scale inhibitor in Experiment 1 was to have a baseline of the behavior of SI under reservoir conditions and with the presence of field brine. In addition, the study of adsorption of the dialyzed scale inhibitor containing only sulfonate onto the sand versus the adsorption of the same solution mixed with sulfate-containing SW was of great interest. This step in the research would yield answers on how sulfate affects the adsorption of SI.

3.4.6.1.3 Experiment 3 –SW Injection

In this part of the investigation, three pore volumes of synthetic sea water (SW) were injected without any scale inhibitor. The same procedure from Experiment1 and Experiment 2 was followed with the mentioned exception. This experiment was the concluding part of a complete study of scale inhibitor adsorption on silica with and without the presence of SW.

3.4.6.1.4 Experiment 4 –5% Dialyzed SI in RO Water Injection

For the last experiment, three pore volumes of 5% dialyzed scale inhibitor diluted in RO water was injected into the sand pack. This procedure is similar to Experiment 1 except that 24 h of shut-in are followed by RO water injection for the displacement process. The rest of the experimental process is the same.

3.4.6.2 Scale Inhibitor Concentration Determination

Scale inhibitor concentrations in effluent samples were determined by ICP-AES. The method of this analytical technique is based on the quantification of sulfur in the effluent samples. A weighed amount of sample was diluted with a known amount of RO water so a simple mathematical ratio could be multiplied by the ICP results to get the actual sulfur concentration, hence the scale inhibitor concentration for the sample. The reasons for the dilution were to reduce salt concentrations to prevent blocking of the nebulizer and to bring sulfur into a measurable range.

Nitric acid (HNO_3) was added to each sample until 2 wt% of HNO_3 was achieved in the solution. Then, the samples were diluted 10 times for sulfur and 100 times for the rest of the minerals studied (Ca, Ba, Mg, Si, and Sr) in RO water. At the beginning of each test a three-point calibration run took place. One RO water sample followed by two sulfur standard samples at different known concentrations were tested. In addition quality control checks took place every 10 samples. The plasma, the auxiliary and nebulizer flow rate were 15 L/min, 0.2 L/min and 0.8 L/min respectively. The viewing position used for sulfur was axial and for the rest of the minerals (Ca, Ba, Mg, Si and Sr) was radial. Table 3.5 describes the wavelength used for all the elements analyzed. The above procedure was performed by Dr. Sheng-Xue Xie and Dr. Karen Peltier. The uncertainty measurement for these elements was +/- 10%.

Table 3. 5 Wavelengths Used for ICP Analysis

Element	Wavelength (nm)
Sulfur	180.669
Barium	455.403
Calcium	393.366
Magnesium	279.553
Silicon	251.611
Strontium	407.771

Chapter 4

Results and Conclusion

In this chapter the results of the experiments are presented and discussed. There are three sets of experiments that address a complete study of the interaction of scale inhibitor SI, field brine (FB), Synthetic Sea Water (SW) and the porous media (silica sand packs). The chapter is divided into four sections. Section 4.1 discusses the pH changes of the effluent samples. Section 4.2 describes the pressure data. Section 4.3 covers the particle size and polydispersity of the displaced material and the UV/Vis absorbance. In addition, turbid effluent samples were subjected to a precipitation study which will be discussed at the end of Section 4.3. Section 4.4 covers the retention that occurred during the porous media injection by analyzing the concentration profile of sulfur in the effluent fluid. Also, at the end of Section 4.4, a discussion on how other minerals affect adsorption will take place by analyzing the concentration profiles of magnesium, calcium, strontium, barium and silicon.

In summary, four experiments were conducted, the first one consisted of injecting 3 pore volumes of dialyzed SI in RO water, which was then displaced by field brine. The second experiment covers the injection of 3 PV of dialyzed SI in SW, displaced by field brine. The third experiment consisted of injecting 3 PV of SW displaced by field brine. Finally, 5% of dialyzed SI in RO water were injected and then displaced by RO water.

4.1 Influence of pH in scale inhibitor adsorption

Figure 4.1 shows the pH values for the effluent samples versus pore volume for experiment 1 (PEEK #1 04/19/10). This experiment consisted of injecting 5% dialyzed SI in RO water which was displaced by field brine after a 24 hour shut-in period. The pH values start to decrease at scale inhibitor breakthrough (1 PV). In addition, this reduction of pH is accentuated after 24 h of shut-in.

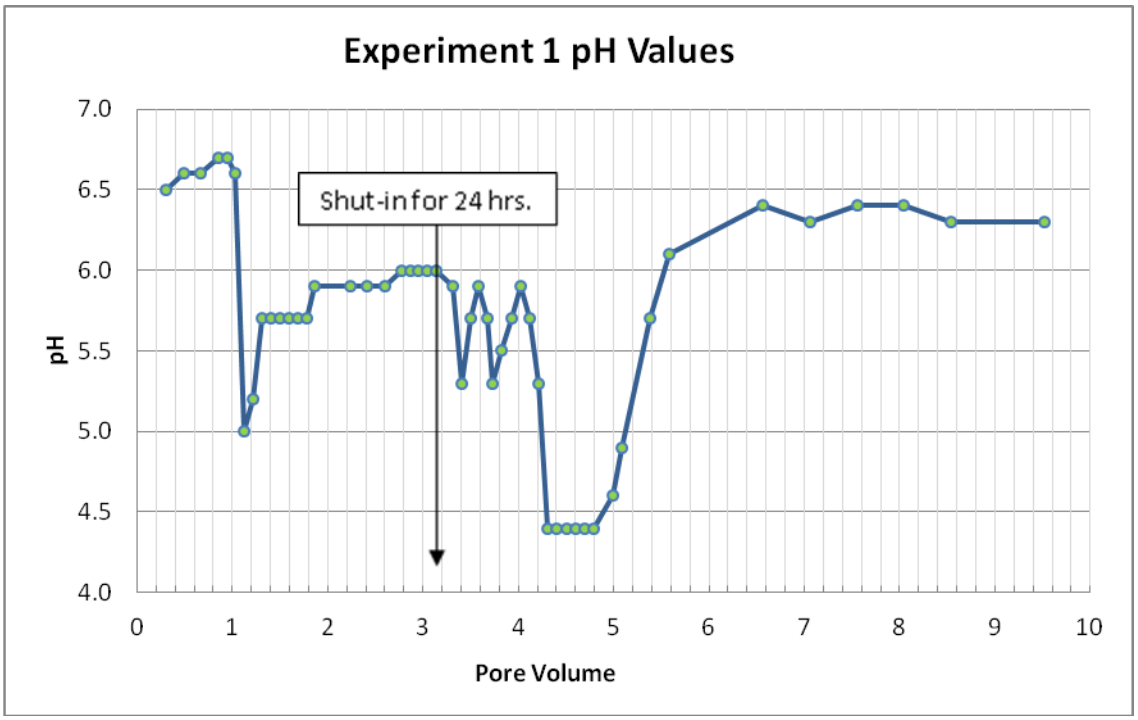

Figure 4. 1 5 % SI in RO water displaced by FB experiment pH Results

The injection of 5% dialyzed SI in SW displaced by field brine was the second experiment (PEEK# 1 05/18/10). Figure 4.2 shows the results of the measured pH values versus pore volume.

The same phenomenon occurs in this experiment, pH values decreased when the scale inhibitor was in contact with the sand and field brine (at PV =1). However, the values stay relatively constant after shut-in.

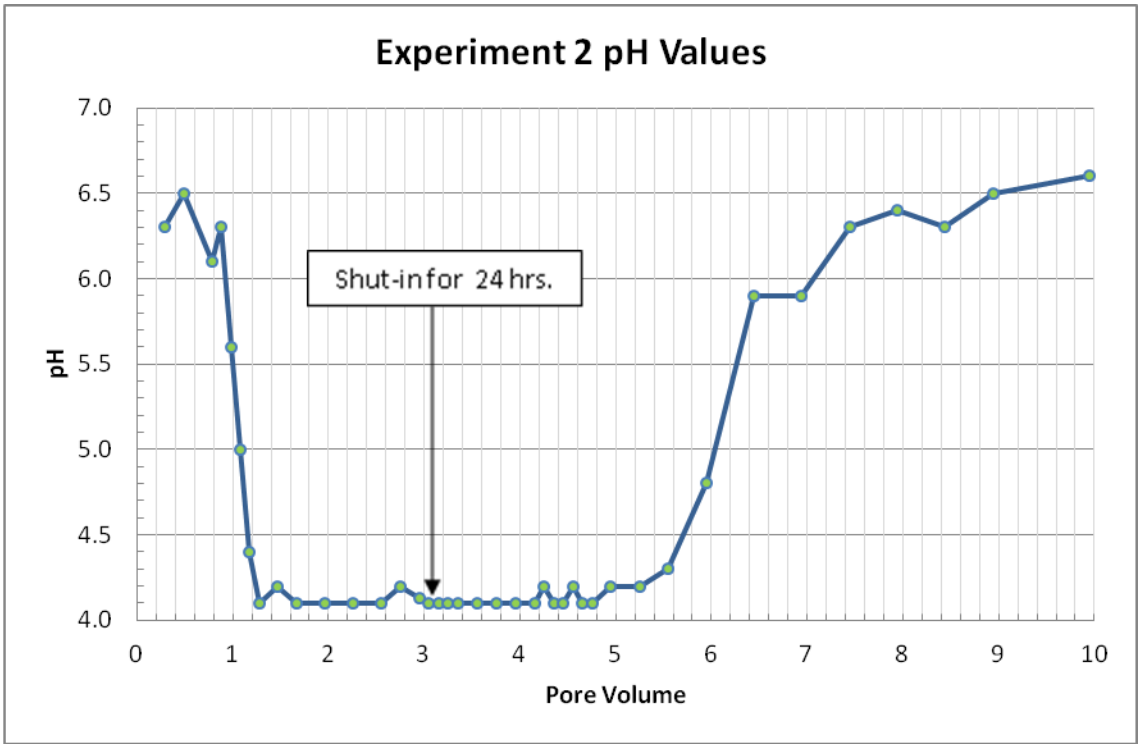

Figure 4. 2 5% SI in SW displaced by FB pH Results

The third experiment, which consisted of injection of only synthetic seawater (SW) and then displaced by field brine, was performed to study the behavior of sea water in the presence of field brine in porous media. Figure 4.3 shows the plot of pH values versus pore volume for this experiment.

Figure 4.3 does not show the immediate reduction of pH at breakthrough (PV=1) as was observed in the previous 2 experiments.

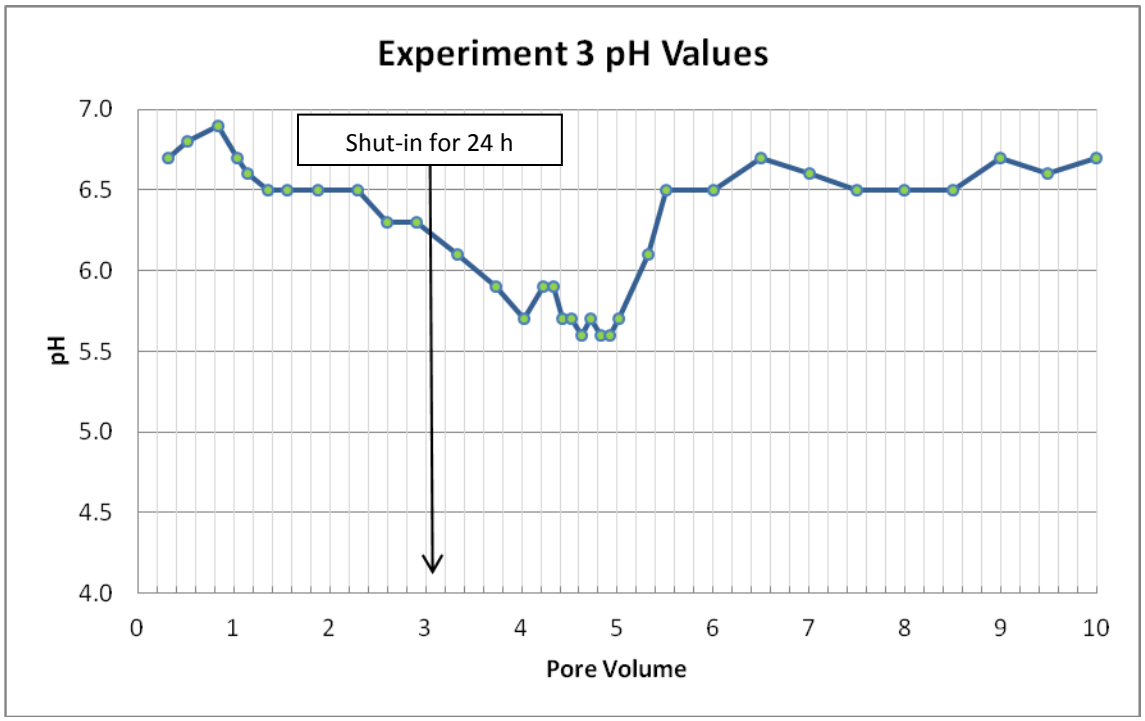

Figure 4. 3 SW injected and displaced by FB pH Results

Finally, for the last experiment, 5% dialyzed SI in RO water was injected, then displaced by RO water. Figure 4.5 depicts the pH results for this experiment.

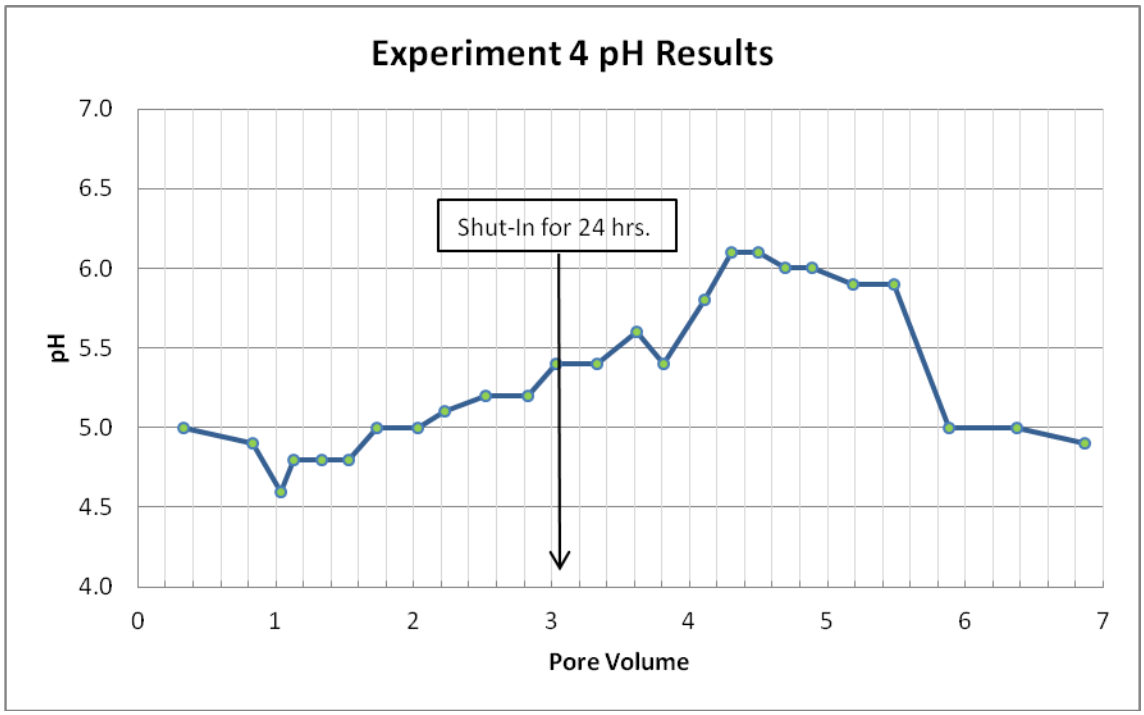

Figure 4. 4 5 % SI in RO water displaced by RO water pH Results

Even though there is a slight reduction of pH after scale breakthrough (PV=1), the values gradually increase after shut-in. This experiment is similar to Experiment 1 except that RO water was used to displace the scale inhibitor instead of field brine. This increment of pH might be due to the absence of the ion interaction that was present in Experiments 1 through 3.

It is known from studies by Laing et al. [13] and Sorbie et al. [23] that the adsorption of PVS scale inhibitors decreases as the pH rises from 2 to 6 when measured in pure water and follow the same pattern between pH 2 and 4 when measured in a calcium-containing sea water. Increasing pH reduces adsorption because of the electrostatic repulsion between the surface and

the inhibitor i.e. both the inhibitor and the quartz surface charge become more negatively charged. In addition, it has been observed that the mechanism of adsorption at pH values greater than four is by electrostatic bridging through calcium ions and not hydrogen bonding. In Section 4.3, the influence of calcium on scale inhibitor adsorption will be discussed in more detail.

The pH data shows that ionic exchange is accentuated when scale inhibitor is in contact with the sand (at PV =1) and especially in the presence of FB and SW. According to literature, adsorption tends to be favorable when pH decreases as it was observed in the experiments.

4.2 Pressure Data Results

Pressure data from the displacement experiments were plotted in Appendix C. A constant pressure drop across each sand pack during the injection experiments is observed. Pressures were slightly disturbed when shut-in occurred (at PV =3) presumably due to a temperature built up overnight and lack of flow. However, when injection was resumed the pressure measurement stabilized and there was no evidence of any permeability change during the displacement experiments.

4.3 UV/Vis absorbance, Particle Size and Polydispersity Results

The in-line absorbance data was collected for each experiment and the results were used as guidance to pinpoint the samples of interest for the ICP analysis. This data was not used to quantitatively measure adsorption; instead, it only gave an idea of where the fluid mixing occurred in terms of pore volume. ICP-AES analysis technique (Section 3.4.6) was used to measure sulfur concentration of the effluent samples. The sulfur concentration results were used to determine adsorption of scale inhibitor. This process will be discussed in Section 4.4.

Figure 4.5 shows that the absorbance data measured at 303 nm exceeded the maximum quantifiable amount by the UV/Vis spectrometer. Therefore, the data has been normalized to the

5% dialyzed SI in RO water as the maximum absorbance and field brine as the minimum absorbance. This plot demonstrates that the effluent material from the displacement test is going under considerable mixing. The sampling frequency was incremented at these points; then these samples were analyzed using the ICP-AES technique. This will be discussed in detail in Section 4.4.

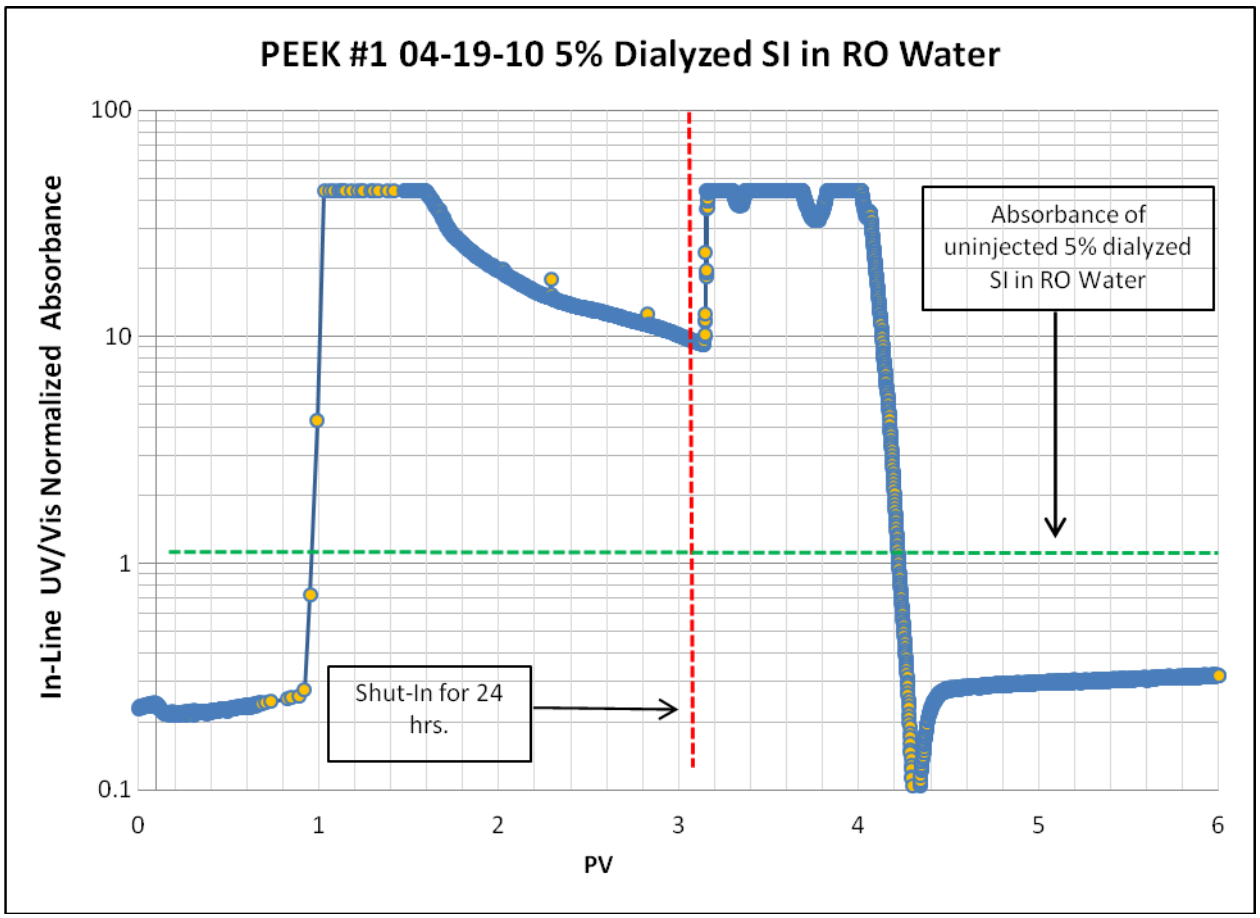

Figure 4. 5 5% SI in RO displaced by FB In-Line Absorbance Results

The same occurs in Figure 4.6 which shows the results from experiment 2. The difference between Experiments 1 and 2 is that the 5% dialyzed SI is diluted in RO water and SW respectively.

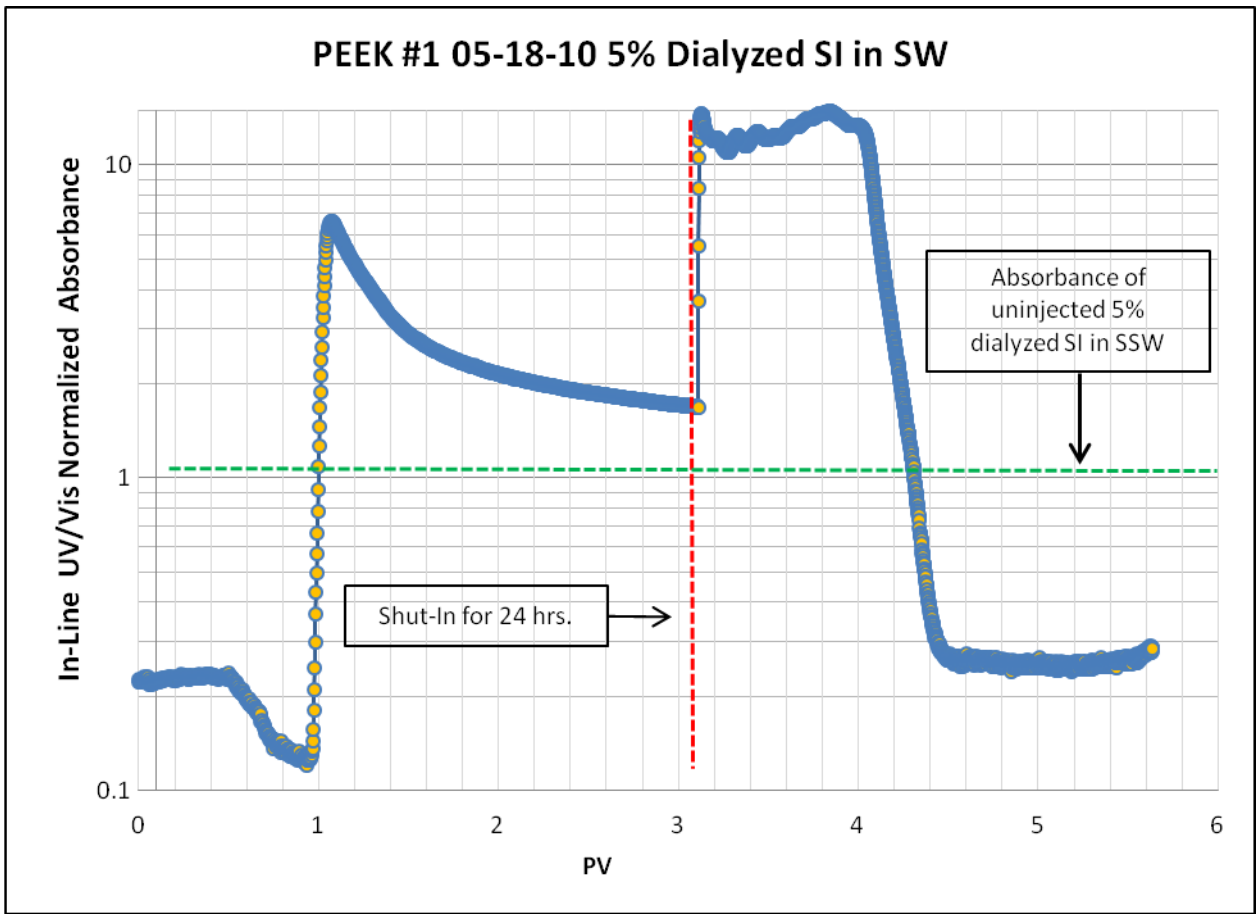

Figure 4. 6 Experiment 2 In-Line Absorbance Results

The third experiment, which differs from the other two because SW was injected instead of scale inhibitor, shows some adsorption characteristics. It is observed that the maximum absorbance of the effluent equals the un-injected absorbance of the fluid in question, in this case being SW. This phenomenon coincides with the ICP results that will be shown in the next section. Figure 4.7 describes the UV/Vis absorbance of Experiment 3, mentioned above.

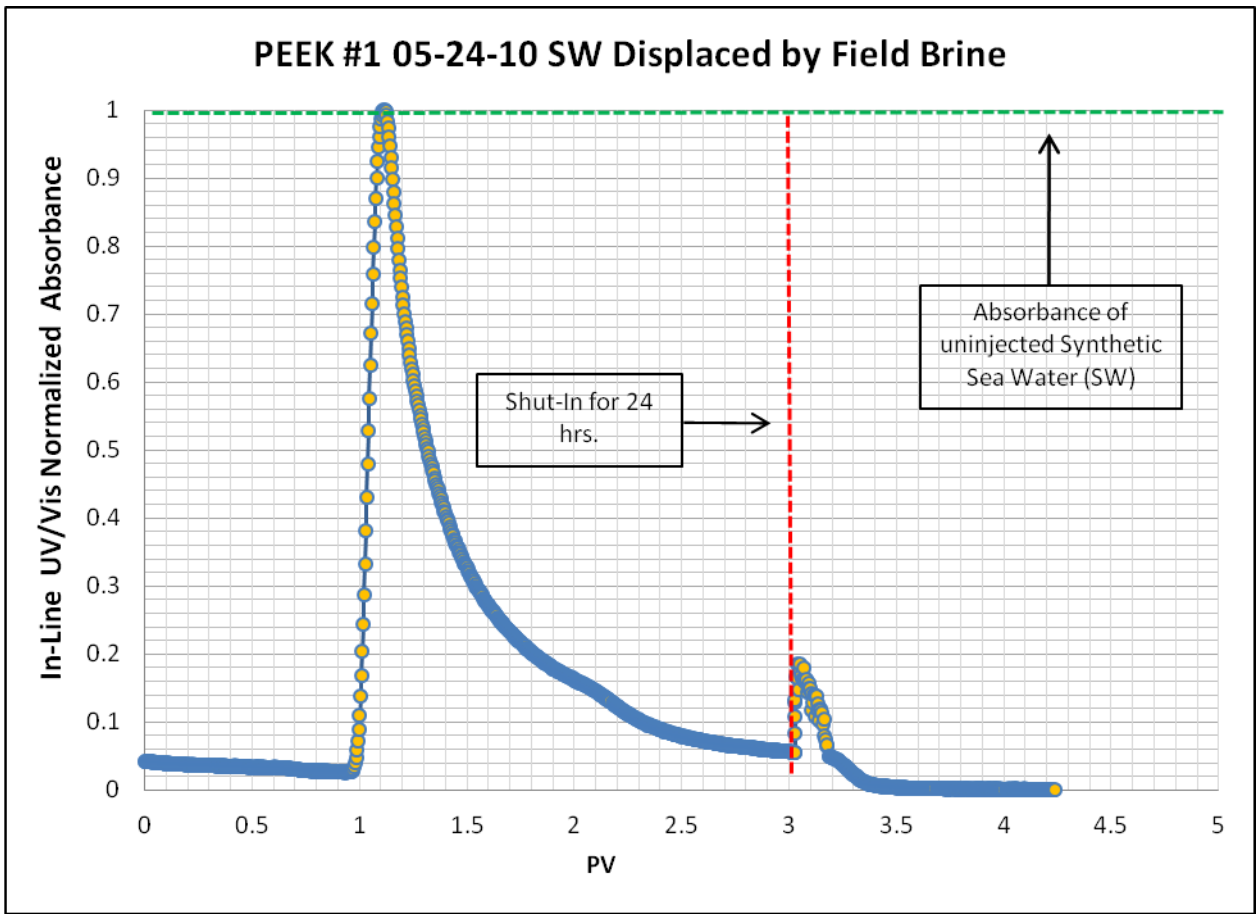

Figure 4. 7 Experiment 3 In-Line Absorbance Results

The last experiment consisted of injecting 5% of SI in RO water, then displacing with RO water. Figure 4.8 illustrates the absorbance results from this experiment. Unlike the previous experiments, significant silica dissolution took place when the scale inhibitor in RO water contacted the sand. ICP-AES analysis confirmed this phenomenon and the results are explained in detail at the end of Section 4.4. In other words, sand mass has been lost during the displacement experiment. This explains the strange shape of the absorbance curve depicted in Figure 4.8.

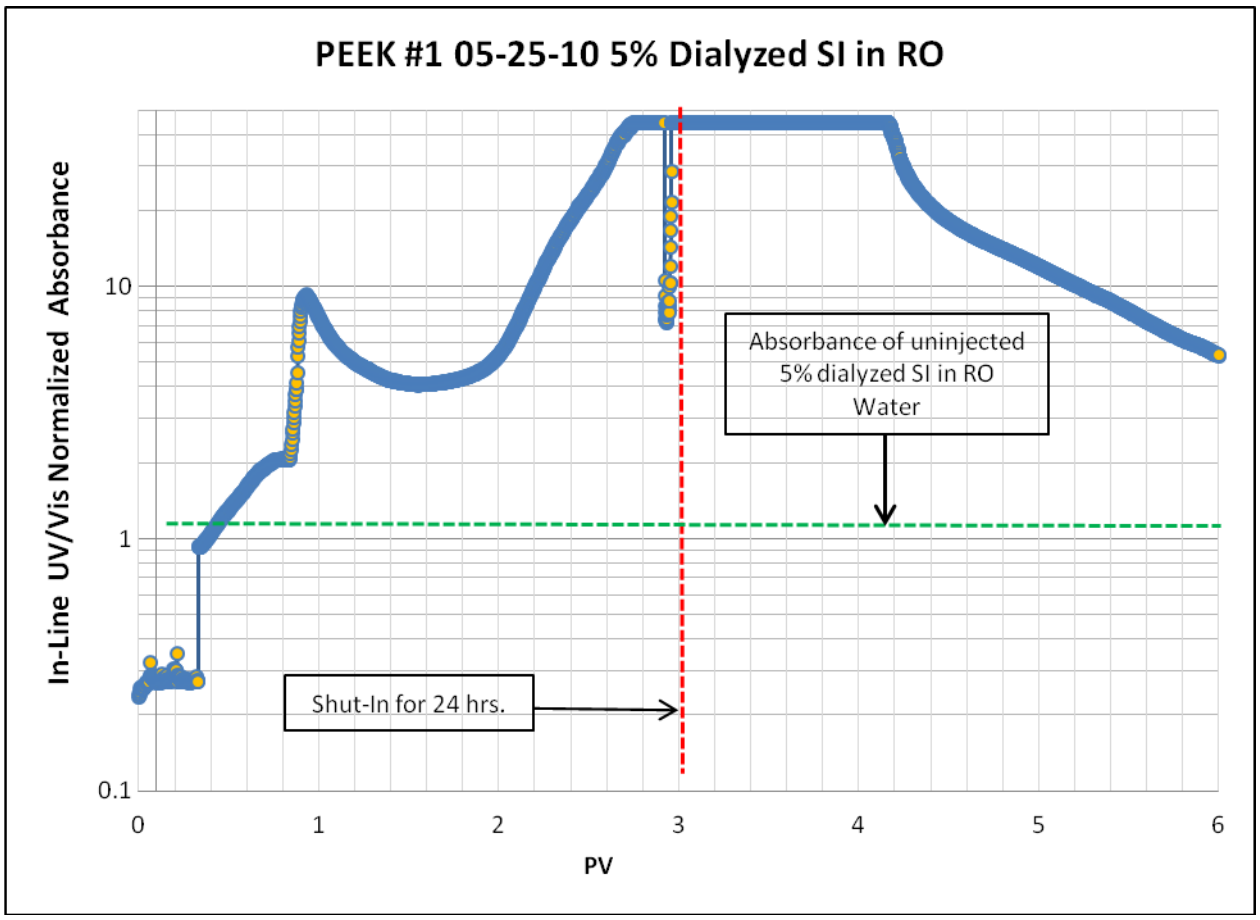

Figure 4. 8 Experiment 4 In-Line Results

Some effluent samples were turbid, indicating the formation of precipitates due to fluid/fluid mixing or fluid/rock interaction. The particle size and polydispersity of the effluent samples for all experiments were measured using the Zeta PALS Particle Analyzer manufactured by Brookfield. The reason for this measurement was to verify whether precipitation was taking place during the displacement experiments.

Table 4.4 describes the particle size and polydispersity results of Experiment 1. The table includes the mean diameter of particles and the count rate. Samples with a count rate of less than 50 are not considered significant. All effluent samples collected after scale inhibitor

breakthrough (at 1 PV) contained turbidity. The particle size and count rate confirmed that particles were formed and had an average size diameter of 385 nm. It appears that particles formed when the scale inhibitor solution displaced field brine from the sand pack.

Table 4. 1 Experiment Particle Size and Polydispersity Results **in Experiment 1** -5% SI in RO Displaced by FB

Sample #	PV	Mean Size Diameter (nm)	Size Standard Dev.	Polydispersity	Polydispersity Standard dev.	Count Rate (kcps)
6	0.574	1031.6	81.1	0.15	0.081	21.1
9	0.849	2185	239.8	0.005	0	30.6
11	1.035	2986	1517.1	0.132	0.127	17.3
12	1.127	686.4	62.8	0.201	0.057	399.9
13	1.220	434.6	15.3	0.238	0.011	421.5
15	1.407	321.8	2.5	0.202	0.021	450
17	1.593	330.4	1.5	0.212	0.022	430
20	1.868	371.6	4.8	0.175	0.021	444
22	2.051	394.2	4.1	0.185	0.021	402.7
25	2.323	408.1	3.7	0.222	0.004	308.7
28	2.595	425.9	2.6	0.225	0.032	346.5
31	2.866	409.2	5.4	0.229	0.013	645.5
34	3.136	406.6	5.1	0.208	0.048	328.5
37	3.405	378.4	2.6	0.205	0.023	432.8
39	3.585	331.5	3.1	0.228	0.012	534.8
42	3.828	359.3	1.8	0.219	0.019	540.3
44	4.020	384.4	5	0.189	0.011	423
45	4.116	388.1	3.2	0.234	0.016	442.1
46	4.214	439.2	4.9	0.214	0.009	334.5
47	4.310	861	29.2	0.255	0.041	442.2
48	4.407	1007.3	64.6	0.287	0.034	218
50	4.600	1159.7	71.9	0.324	0.033	429.4
53	4.893	2123.5	1371.4	0.438	0.222	30.1
56	5.188	3207.1	1945.8	0.614	0.044	15

Experiments 2 and 3 did not show particles. The count rate was less than 30 for most samples and the standard deviation of the mean size diameter exceeded the accepted error range. Tables 4.2 and 4. 3 describe the mentioned results.

Table 4. 2 Experiment 2- Particle Size and Polydispersity -5% SI in SW Displaced by FB

Sample #	PV	Mean Size Diameter (nm)	Size Standard Dev.	Polydispersity	Polydispersity Standard dev.	Count Rate (kcps)
3	0.291	1441.9	398.7	0.134	0.129	21.0
8	0.781	1604.1	377.2	0.131	0.126	8.8
10	0.978	1036.8	209.7	0.486	0.033	7.5
11	1.076	1007.6	418.8	0.492	0.056	5.1
12	1.174	1036.6	206.8	0.359	0.047	6.6
13	1.273	1175.5	397.5	0.005	0.000	13.8
14	1.372	937.2	316.4	0.360	0.042	20.3
17	1.667	1283.5	124.1	0.286	0.147	21.7
20	1.961	512	256.1	0.291	0.145	5.6
23	2.257	1101.1	249.9	0.212	0.105	13.4
26	2.553	5459.9	3258	0.453	0.144	7.2
30	2.948	474.1	126.3	0.154	0.149	14.7
33	3.249	3518.9	2477.1	0.456	0.048	6.7
36	3.548	5860	4243	0.163	0.158	13.8
40	3.950	717.9	183.4	0.230	0.113	9.8
43	4.254	1612.9	488.1	0.005	0.000	23.7
45	4.454	1283.3	219.3	0.317	0.156	20.5
48	4.752	985.9	312	0.124	0.119	16.4
50	4.950	4280.5	3007	0.363	0.191	8.9
53	5.248	2065.9	28.6	0.005	0.000	26.6
56	5.548	2758	1645.2	0.314	0.309	22.1
60	5.948	1736	1543	0.198	0.193	14.5
65	6.442	772	158.3	0.245	0.130	17.2
70	6.941	3156	3069.7	0.281	0.142	18.1

Table 4. 3 Experiment 3 Particle Size and Polydispersity-SW displaced by FB Experiment Particle Size and Polydispersity

Sample #	PV	Mean Size Diameter (nm)	Size Standard Dev.	Polydispersity	Polydispersity Standard dev.	Count Rate (kcps)
3	0.310	1441.9	398.7	0.134	0.129	21
8	0.831	1604.1	377.2	0.131	0.126	8.8
10	1.143	1036.8	209.7	0.486	0.033	7.5
11	1.248	1007.6	418.8	0.492	0.056	5.1
12	1.352	1036.6	206.8	0.359	0.047	6.6
13	1.457	1175.5	397.5	0.005	0	13.8
14	1.561	937.2	316.4	0.36	0.042	20.3
17	1.769	1283.5	124.1	0.286	0.147	21.7
20	2.082	512	256.1	0.291	0.145	5.6
23	2.393	1101.1	249.9	0.212	0.105	13.4
26	2.704	5459.9	3258	0.453	0.144	7.2
30	3.117	474.1	126.3	0.154	0.149	14.7
33	3.331	3518.9	2477.1	0.456	0.048	6.7
36	3.629	5860	4243	0.163	0.158	13.8
40	4.029	717.9	183.4	0.23	0.113	9.8
43	4.327	1612.9	488.1	0.005	0	23.7
45	4.525	1283.3	219.3	0.317	0.156	20.5
48	4.822	985.9	312	0.124	0.119	16.4
50	5.019	4280.5	3007	0.363	0.191	8.9
53	5.316	2065.9	28.6	0.005	0	26.6
56	5.613	2758	1645.2	0.314	0.309	22.1
60	6.008	1736	1543	0.198	0.193	14.5
65	6.502	772	158.3	0.245	0.13	17.2
70	6.999	3156	3069.7	0.281	0.142	18.1

Table 4.4 presents particle size measurements for Experiment 4. Results are similar to Experiment 1 in terms of particle size and count rate.

Table 4. 4 Experiment 4- Particle Size and Polydispersity -5% SI in RO water displaced by RO water

Sample #	PV	Mean Size Diammeter (nm)	Size Standard Dev.	Polydispersity	Polydispersity Standard dev.	Count Rate (kcps)
3	0.329	5369.1	2808.4	0.582	0.352	18.8
8	0.830	27064	20522	0.411	0.253	6.8
10	1.032	343.1	11.2	0.207	0.024	129.4
11	1.130	362.2	29.6	0.204	0.022	94.2
13	1.331	347.3	7.2	0.246	0.014	99.4
15	1.530	401.4	30.5	0.163	0.063	203.9
17	1.728	361.3	7.1	0.246	0.024	230.0
20	2.026	358.4	19.5	0.191	0.024	271.2
22	2.223	314	5.6	0.134	0.012	482.2
25	2.523	372.8	4.3	0.210	0.032	406.5
28	2.825	395.1	4.2	0.207	0.029	510.7
31	3.034	450.8	8.4	0.189	0.030	431.5
34	3.324	353.6	2	0.179	0.034	430.3
37	3.617	380.3	8.4	0.240	0.008	430.5
39	3.812	297.4	4.5	0.150	0.005	474.4
42	4.107	417.3	11	0.196	0.015	498.1
44	4.306	460.1	3.2	0.140	0.012	443.1
46	4.499	430	1.5	0.173	0.024	384.5
48	4.696	472.4	12	0.220	0.026	342.6
50	4.892	374.1	2.6	0.189	0.029	407.3
53	5.188	470.7	9	0.239	0.023	370.1
56	5.485	470	6.5	0.261	0.016	486.2
60	5.877	541.3	23.9	0.23	0.037	408.6
65	6.370	418.7	1.2	0.171	0.033	385.6
70	6.862	420.5	17.4	0.266	0.008	422.4

Interestingly, Experiments 1and 4 yielded a range of particles that were formed during the displacement process. An effort to identify the precipitated particles was made and the results will be discussed in Section 4.5.

Particles were found in the effluent in Experiments 1 and 4. Two effluent samples from Experiment 1 were selected for further analysis to determine the composition of the particles. Samples 16 (1.5 PV) and 13 (2.86 PV) from Experiment 1were centrifuged for 90 minutes at 16,000 RPM. Solids centrifuged from the solutions were collected in a pellet that formed at the bottom of each centrifuge tube. The ICP was used to determined concentrations of the supernatant and the pellet after centrifugation. The pellet was dissolved with 1 M HCl and diluted 10 times the original volume with RO water in order to determine concentrations. Table 4.5 shows the results of this side study. The pellet contained sulfur and silicon suggesting that the precipitate was composed of silica and PVS. Silica was dissolved from the sand by the injected fluids.

Table 4. 5 Experiment 1 Centrifuged particles Analysis for sample 16 and 31

	S (mg/L)	Ca (mg/L)	Mg (mg/L)	Ba (mg/L)	Sr (mg/L)	Si (mg/L)
Sample 16 Untreated	322	3.08	4.29	2.44	0.695	4.34
Supernatant 1 (top)	310	3.62	2.19	2.37	0.301	3.78
Supernatant 2 (bottom)	320	4.33	6.76	2.63	0.727	3.62
Dissolved Pellet*	28.7	2.85	1.96	0.345	0.509	24
Sample 31 Untreated	276	0.743	0.906	0.548	0.170	4.00
Supernatant 1 (top)	270	1.07	1.81	0.550	0.284	2.91
Supernatant 2 (bottom)	276	1.16	0.599	0.512	0.0789	3.18
Dissolved Pellet*	18.10	0.1090	0.0727	0.0000	0.0545	39.6

*Note: Concentrations in the dissolved pellet are estimates, assuming the volume of sample used to create the precipitate was 2mL. Untreated samples means before centrifugation.

4.4 Scale Inhibitor Adsorption

The primary objective of this thesis was to study the adsorption of the commercial scale inhibitor SI on silica sand. The analytical technique used in determining adsorption was ICP-AES, which consisted of measuring the amount of sulfur present in the effluent samples for each displacement experiment. Therefore, any source of sulfur of any form in the system would alter the concentration results significantly. Figure 4.9 shows the concentration profile of the effluent samples for Experiment 1, which consisted of injecting 3 pore volumes of 5% dialyzed SI in RO water and then displacing with field brine.

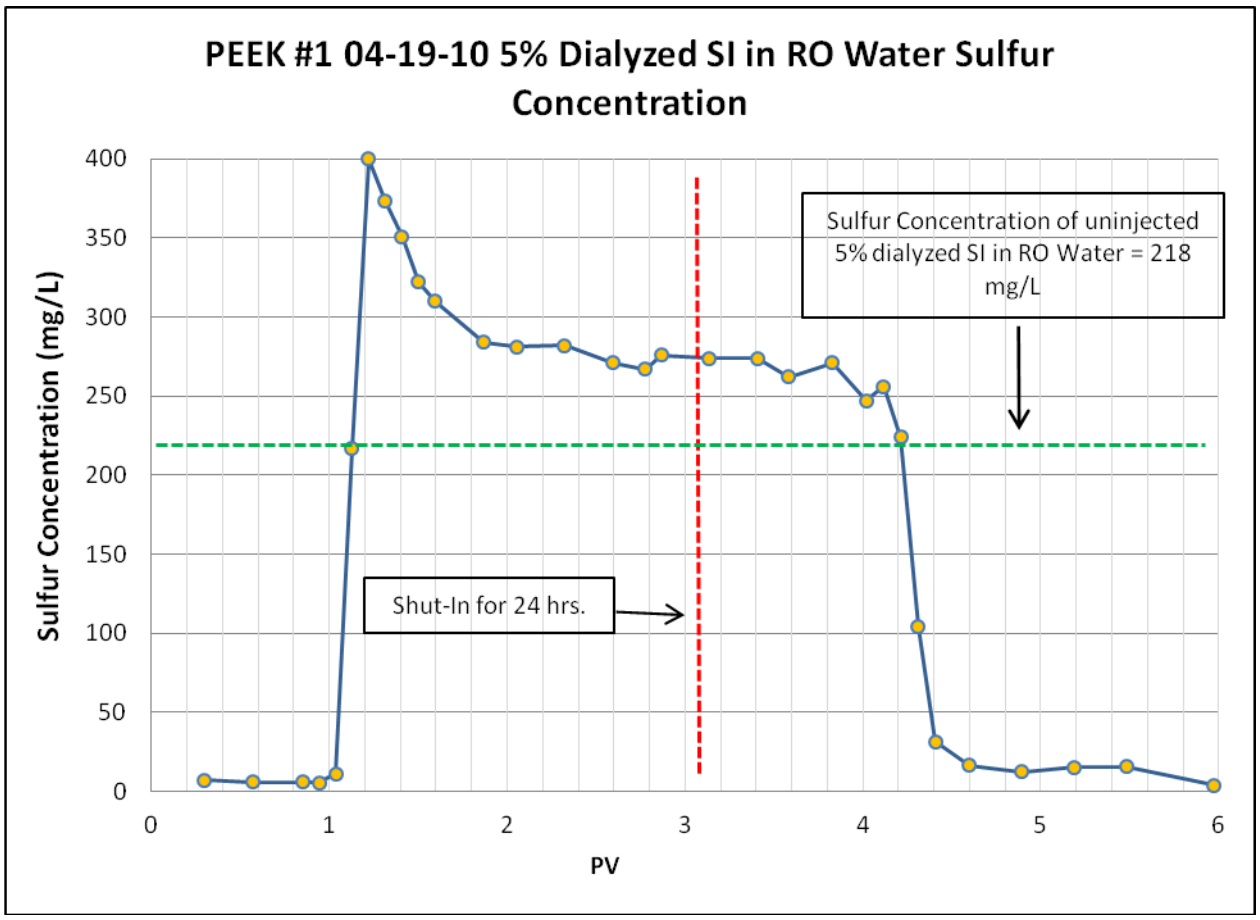

Figure 4. 9 Sulfur concentration in the effluent samples from Experiment 1- 5% SI in RO water Displaced by FB

The sulfur concentration is greater than the initial un-injected concentration. This means that the uncertainty in analyzing sulfur in effluent samples that have contacted silica sand at 70˚C is significant. The uncertainty in determining sulfur concentration in the range of 250 ppm using the ICP was estimated to be 25 ppm. Since this uncertainty does not resolve the problem of excess sulfur concentration in the effluent, there is a possibility that another constituent is interfering with the analysis for sulfur. Table 4.6 shows the pre and post-injection sulfur concentration for Experiment 1.

Table 4. 6 5% SI in RO water displaced by FB Experiment Scale Inhibitor Adsorption Results

Scale Inhibitor In (g)	Scale Inhibitor Out (g)	Scale Inhibitor Retained (g)
0.0696	0.0906	-0.0210

Figure 4.10 shows the sulfur concentrations of Experiment 2. This displacement test was performed by injecting of 3 pore volumes of 5%SI in SW, and then displaced by field brine. The sulfur concentration of SW and the scale inhibitor in SW were measured prior to injection. They are 1028 mg/L and 1057 mg/L respectively. These results demonstrate that ICP is not able to detect the sulfur due to scale inhibitor. The difference between sulfur from SI and sulfur from SW is approximately 2% which is less than the ICP analytical error (10%). The reason for a consistent material balance in this case is the presence of SW in the system, which contains a large amount of sulfur compared to the scale inhibitor (Experiment 1 and 4). This is similar to the results from Experiment 3.

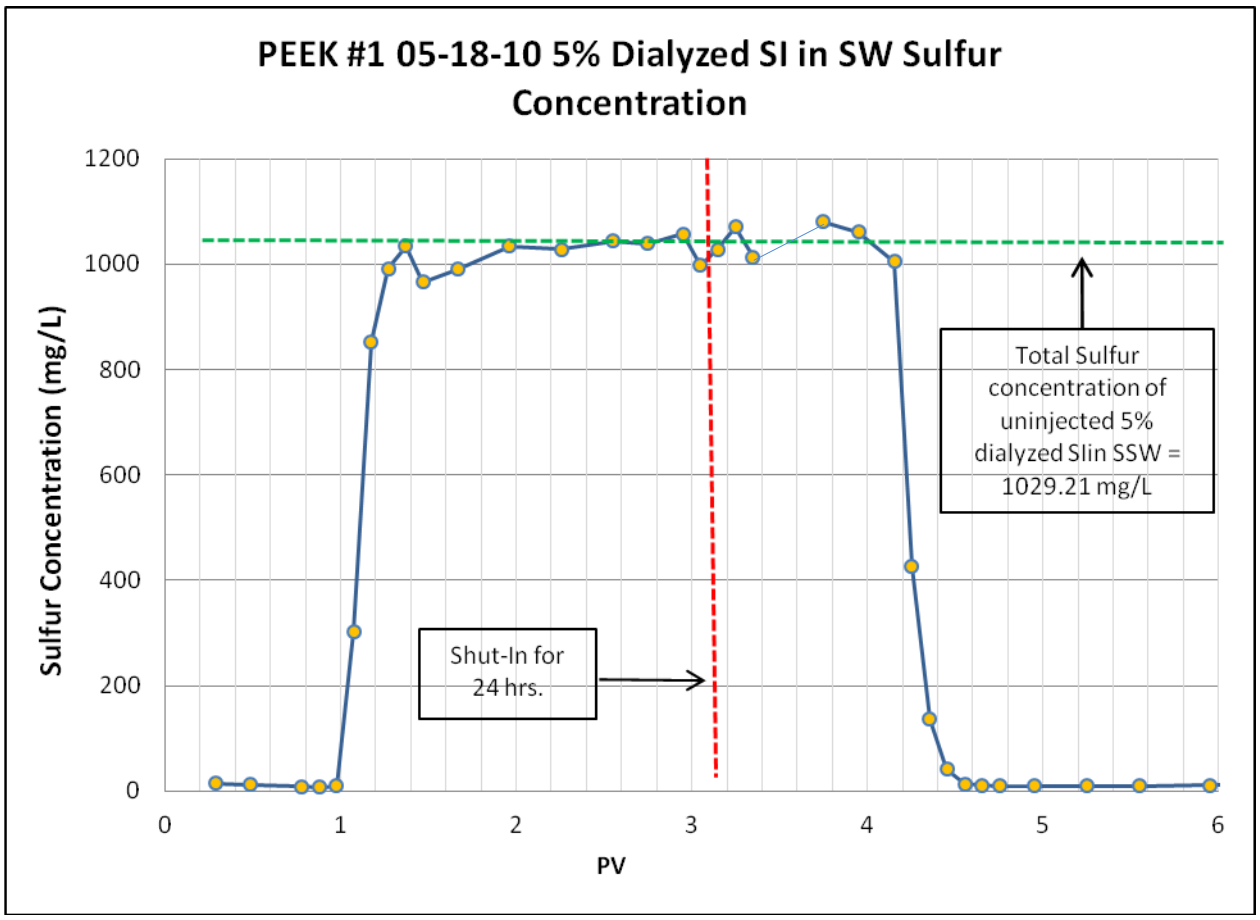

Figure 4. 10 Experiment 2 Sulfur Concentration 5% SI in SW displaced by FB Experiment

Table 4.7 contains the material balance calculation for Experiment 2. The sulfur concentration material balance is consistent, which shows a small scale inhibitor retention detected (0.96 µg/g rock). This small adsorption is negligible.

Table 4. 7 Scale Inhibitor Adsorption in Experiment 2 5% SI in SW displaced by FB Experiment Results

Scale Inhibitor In (g)	Scale Inhibitor Out (g)	Scale Inhibitor Retained (g)	Scale Inhibitor Retained (µg/g rock)
0.3257	0.3253	0.0005	0.9598

Experiment 3 was designed to determine the interaction between SW, field brine and the porous medium. Three pore volumes of SW containing SI were injected and then displaced by field brine. SW stabilizes material balance because of the large amount of sulfur present in SW compared to the sulfur present in SI. The sulfur concentration of SW was 1052 mg/L. Table 4.8 describes the material balance calculation for this experiment and Figure 4.11 shows the sulfur concentration profile.

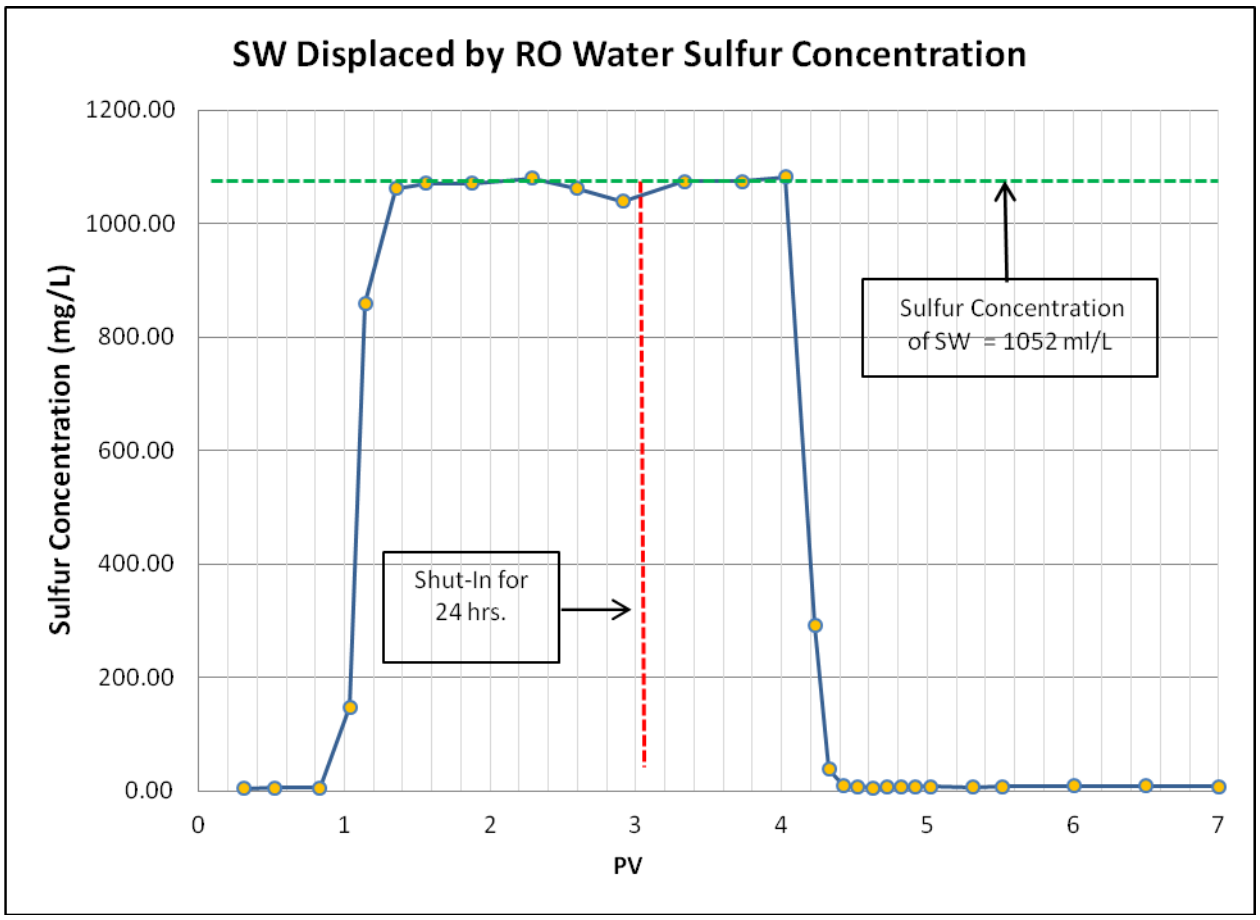

Figure 4. 11 Sulfur Concentration in Experiment 3- SW Displaced by FB –no Si inhibitor

Table 4. 8 SW Displaced by FB Experiment 3 Scale Inhibitor Adsorption Results

Scale Inhibitor In (g)	Scale Inhibitor Out (g)	Scale Inhibitor Retained (g)
0.3216	0.3257	-0.0040

Experiment 4 was performed to study the interaction of only scale inhibitor with the porous media. The experimental procedure and data collection were identical to Experiment 1 except that RO water was used to displace the inhibitor instead of field brine.

Results are similar to Experiment 1 with effluent concentrations exceeding the influent concentrations. Table 4.9 shows the material balance results and Figure 4.12 describes the sulfur profile for Experiment 4.

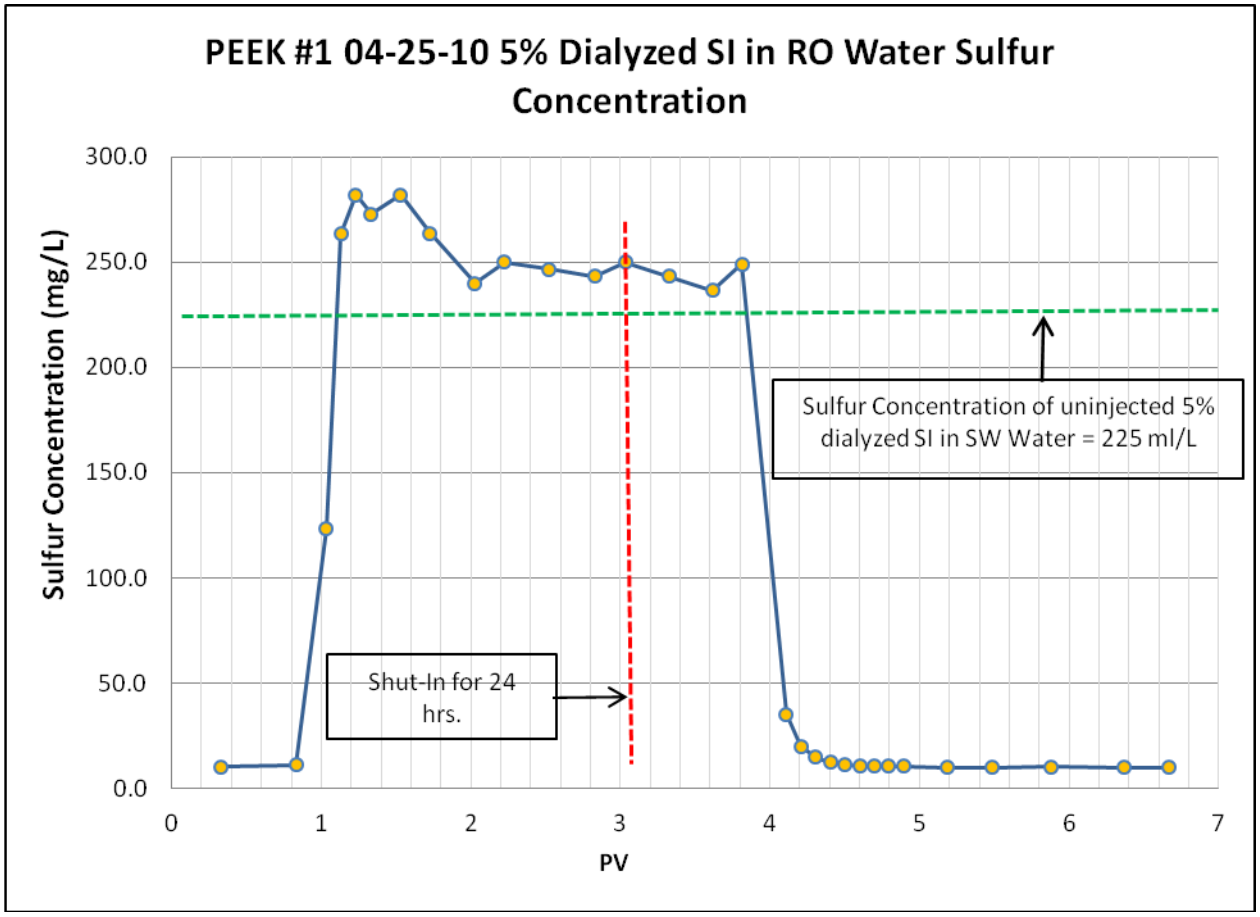

Figure 4. 12 Sulfur Concentration in Experiment 4 5% SI in RO Water Displaced by RO Water

Table 4. 9 5% SI in RO Water Displaced by RO Water Experiment Scale Inhibitor Adsorption Results

Scale Inhibitor In (g)	Scale Inhibitor Out (g)	Scale Inhibitor Retained (g)
0.0666	0.0783	-0.0117

It was observed by Laing [3] that calcium, which is present in both SW and field brine, contributes to an increase of scale inhibitor adsorption in silica through complexation. In the same way as sodium might interact with the scale inhibitor, calcium reduces the negative charge on the polymer, making it easier for them to approach the negatively charged surfaces of the porous media. This behavior creates a more adsorption friendly environment according to the literature.

In addition, according to a study performed by Boak et al. [14] PVS displayed an inhibiting efficiency increase of 18% when Mg concentration was increased. Interestingly, the authors also discovered that increasing magnesium concentration from zero to 1000 ppm in the absence of calcium had a detrimental effect on phosphonate performance, while PVS efficiency increased. However, in general, as discussed earlier, higher calcium concentrations led to improved performance for all inhibitors tested. SW contains 95% more magnesium and 62% more calcium than field brine. Thus, an increment of effluent Mg and Ca concentration is observed in Experiment 3, where SW is displaced by field brine. Neither Experiment 1 nor Experiment 4 displays the same phenomena.

The data from the four experiments demonstrate that uncertainties in the analysis technique limit the determination of adsorption of SI on silica sand. No adsorption was observed within the accuracy of the analysis..

Figure 4.13 describes the concentration profile of 5 elements that were measured using the ICP-AES: barium, strontium, calcium, magnesium and silica. The graph for Experiment 1, which consisted of injecting 3 PV of 5% SI in RO water, later displaced by field brine, demonstrates that there is a sudden drop of elements concentration present in the field brine solution. This occurs when the scale inhibitor is contact with the field brine-saturated sand pack (at scale inhibitor breakthrough).

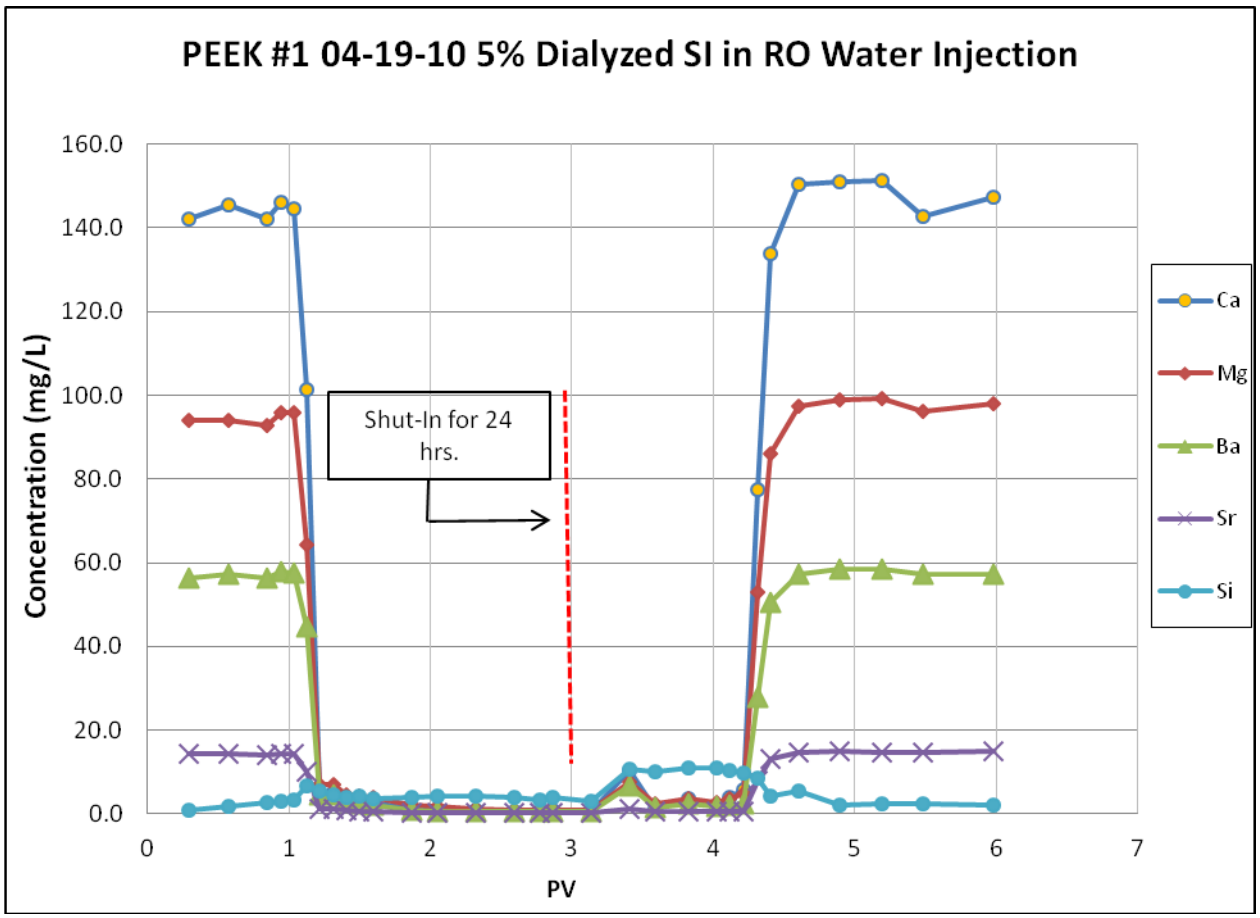

Figure 4. 13 5% SI in RO Water Displaced by FB Ca, Mg, Ba, Si and Sr Concentration results

However, Figure 4.14 depicts the concentration results for Experiment 2 which are clearly different from Experiment 1. Experiment 2 consisted of injecting 3 pore volumes of 5% SI in SW and then displacing with field brine.

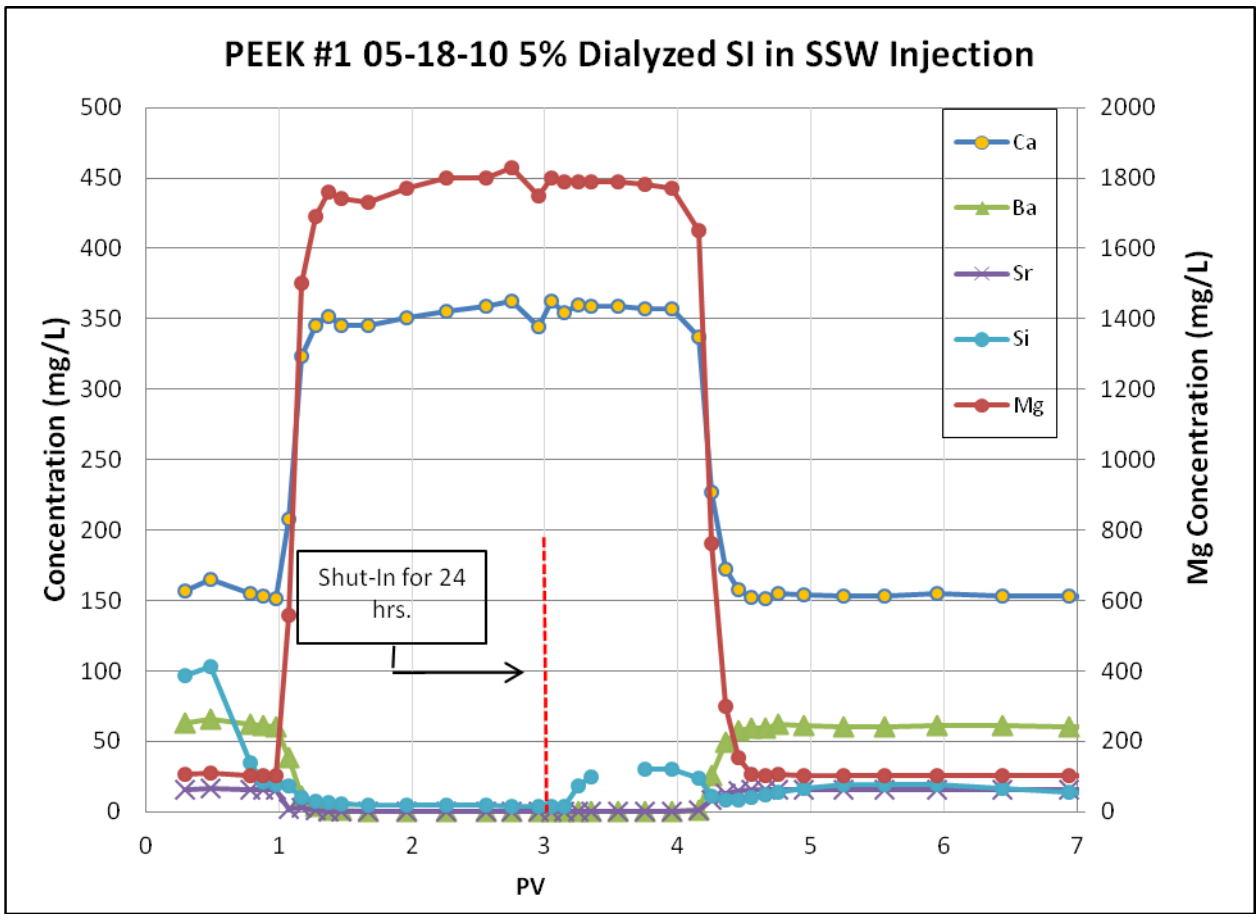

Figure 4. 14 5% SI in SW Displaced by FB Ca, Mg, Ba, Si and Sr Concentrations Results

Furthermore, a reduction in barium concentration is observed at scale inhibitor breakthrough (around 1 PV), which might be a result of $BaSO_4$ precipitation caused by the comingling of field brine and SW, or simply the displacement process. Silicon concentration slightly increases after shut-in, a phenomenon observed in all experiments. Silica dissolution is common in silica sand displacement experiments. Cook [15] witnessed silica dissolution of 3 order of magnitude when characterizing a polymer using silica sand pack displacement tests.

Figure 4.15 demonstrates the concentration results of the same 5 elements for Experiment 3. Three pore volumes of SW were injected followed by field brine in this experiment. The graph depicts an increase of magnesium and calcium concentration. However, since scale inhibitor is absent, the sulfur material balance is consistent with no trace of adsorption (Table 4.9). The increase of silicon concentration after shut-in is also present in this experiment.

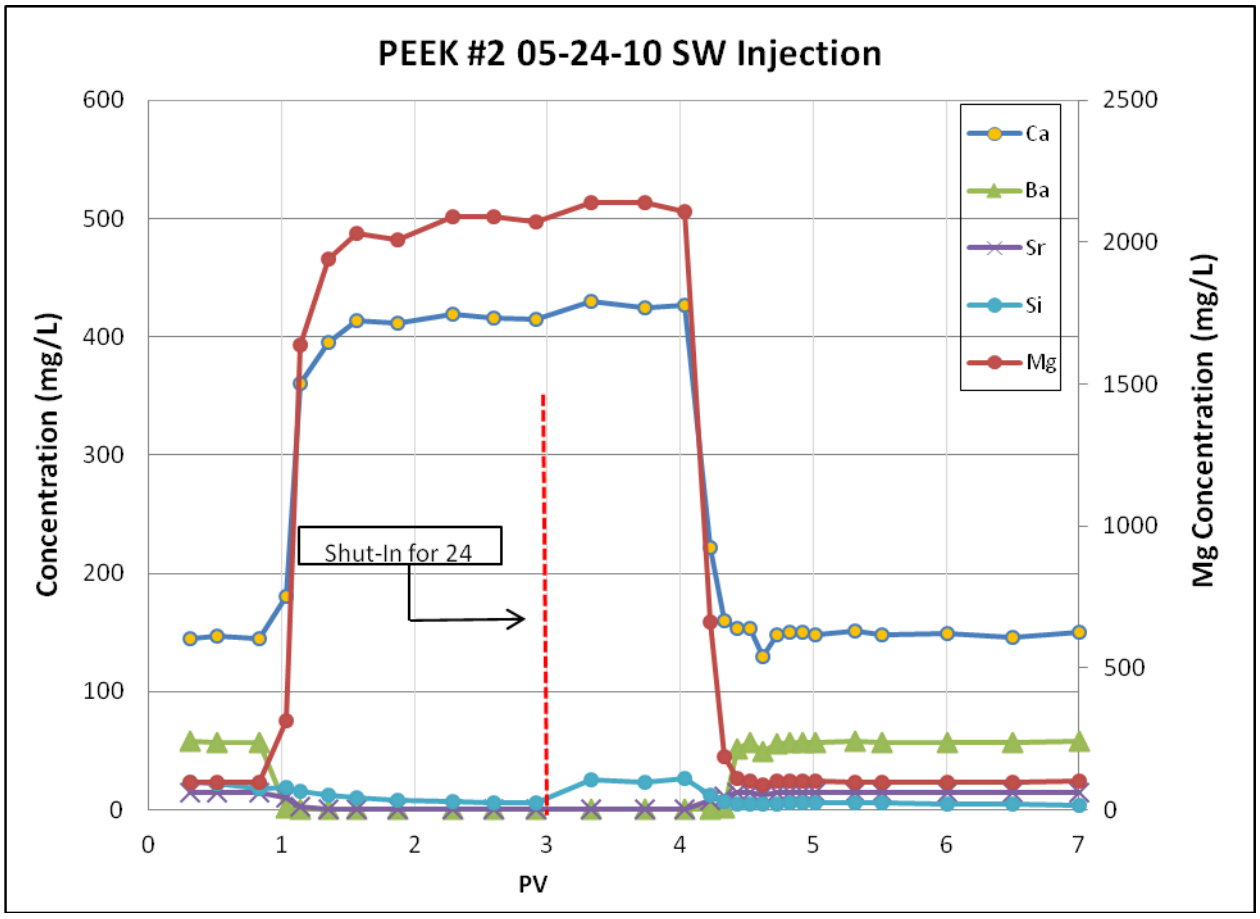

Figure 4. 15 SW Displaced by RO Water Ca, Mg, Ba, Si and Sr Concentrations Results

This increase of silicon concentration in the effluent is more accentuated in Experiment 4.

Figure 4.16 illustrates this phenomenon. It appears that the dissolution of silica interferes with the analysis of sulfur using ICP. Measurement of adsorption of SI on silica sand will require development of an accurate analytical technique.

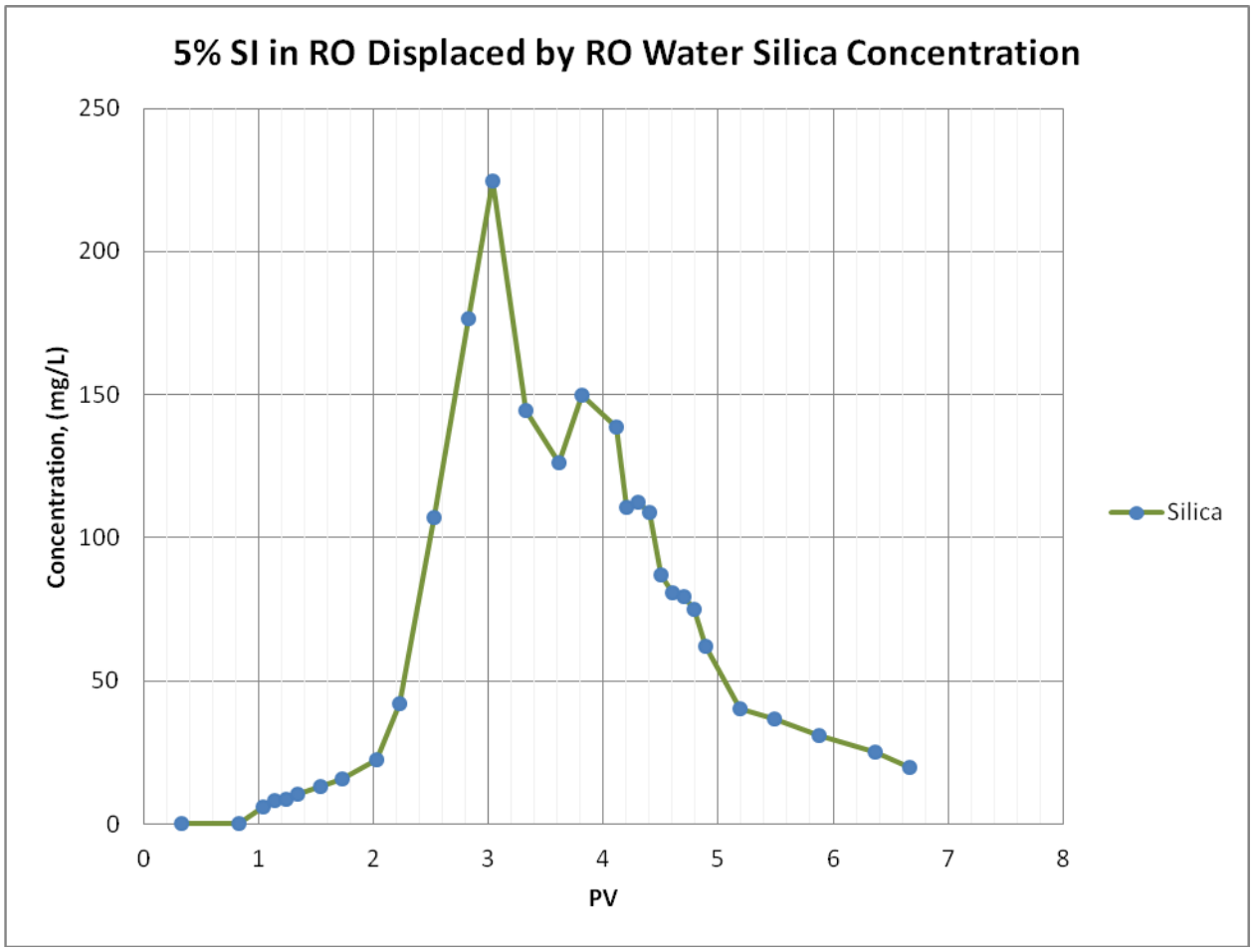

Figure 4. 16 5% SI in RO Displaced by RO Water Silica Concentration Results

In summary, Laing [3] documented how the presence of calcium ions positively influences scale inhibitor adsorption on silica (Section 2.4.2.2). Furthermore, Boak et al. [14] noted that higher salinities reduce the double layer thickness around the scale inhibitor allowing

a closer approach of the inhibitor to the scale surface. This bridging effect is greatly responsible for the increase of scale inhibitor adsorption on silica [22]

Even though it is documented in literature that the presence of calcium and higher salinities enhance the tendency for adsorption to occur, we have been unable to demonstrate adsorption of SI on silica sand due to the analytical technique limitation discussed above.

Chapter 5

Conclusion and Recommendations

5.1 Conclusions

- The ICP-AES analytical technique accuracy limits the determination of adsorption of scale inhibitor on silica sand at 70 °C.
- Silica dissolution occurs when scale inhibitor is in contact with the sand and it is pronounced in the absence of dissolved ions that are present in field brine and SW. This formation of silica-scale inhibitor complex particles was observed in Experiments 1 and 4 where turbid samples were collected and analyzed.
- Since the ICP-AES measuring uncertainty does not fully resolve the sulfur material balance problem, there is a possibility that another constituent, whether in the field brine or silica dissolved from the sandpack, is interfering with the analysis for sulfur.

5.2 Recommendations

- A different analytical technique to accurately determine adsorption of scale inhibitor such as Total Organic Carbon (TOC) for carboxylic acids detection should be used.
- ICP sulfur wavelength range studies should be performed and possibly use another wavelength to improve scale inhibitor sulfur concentration measurement accuracy.
- Oxidation of samples is also suspected to be a reason for the analytical technique problem; therefore, a reduction chemical process applied to the samples prior to ICP analysis might solve this issue. The idea is to force all the sulfur to be in the same oxidation state.

Abbreviations and Nomenclature

ΔG	Surface Free Energy of the Crystal
ΔG_{ads}	Adsorption Entropy
ΔH_{ads}	Adsorption Enthalpy
Γ_{max}	Maximum Adsorption of Scale Inhibitor on Silica (mg/g)
Abs290	Optical Absorbance at 290 nm
AC	Alternating current
BCF	"Burton, Cabrera and Frank"
DC	Direct current
DETPMP	Diethylenetriamine Penta Methylenesphosphonic Acid
FB	Field Brine
FEP	Fluorinated Ethylene Propylene
ICP-AES	Inductively-Couple Plasma Atomic Emission Spectrometry
ID	Inside diameter
K_{eq}	Equilibrium Constant (for an ideal system)
K_{sp}	Solubility Product
MIC	Minimum Inhibitory Concentration
MSDS	Material Safety Data Sheet
Mw	Weight average molecular mass
OD	Outside diameter
PEEK	Poly-ethyl-ethyl-ketone
ppm	Parts per million
PV	Pore Volume

PVS	Polyvinyl Sulfonate
RO	Reverse Osmosis
SI	Scale Inhibitor
S_{ind}	Saturation Index
SR	Saturation Ratio
SW	Synthetic Seawater
T	Temperature, K
t_{ind}	Induction Time
USD	United States Dollar
UV/Vis	Ultraviolet/visible absorbance detector

References

1. Frenier, W.W. and Ziauddin, M., *Formation, Removal, And Inhibition of Inorganic Scale in the Oil Field Environment*. 2008, Richardson, Texas: SPE. 230.
2. CRC *Handbook of Chemistry and Physics - 69th Edition. Editor in Chief R. C. Weast, CRC Press Inc, Boca Raton, FL,* 1988.
3. Laing, N., *The Performance and Mechanisms of Selected Barium Sulphate Scale Inhibitors Under Various Conditions of Brine Composition and Temperature*, in *Petroleum Engineering*. 2006, Heriot Watt University: Edinburgh, Scotland.
4. Mullen, J.W., *Crystallization*. 3rd ed. 1993: Butterworth-Heinemann. 173.
5. Tomson, M. B., Kan, A. T and Fu, G., *Control of Inhibitor Squeeze Through Mechanistic Understanding of Inhibitor Chemistry.* SPE, 2004(87450-PA): p. 283-293.
6. Gill, J.S., *Developments of Scale Inhibitor.* NACE International Corrosion 1996(229).
7. Mackay, E. J., Graham, G. M., *A Background to Inorganic Scaling-Mechanism Formation and Control.* 2004 SPE Formation Damage Symposium, Lafayette, Louisiana, 2004.
8. Sorbie, K. and Graham, G. M., *The Effect of Molecular Weight on the Adsorption/Desorption Characteristics of Polymeric Scale Inhibitors on Silica Sand and in Sandstone Cores.* NACE International Corrosion, Houston, TX, 1994.
9. Breen, P. J., Diel, B. N. and Downs, H. H., *Correlation of Scale Inhibitor Structure with Adsorption Thermodynamics and Performance of Barium Sulfate in Low-pH Environments.* Society of Petroleum Engineers, 1990(SPE 20688): p. 26.
10. Naono, H., *The Effect of Triphosphate on the Crystallization of Strontium Sulfate*. Bulletin of Chemical Society of Japan. 1967. 40: p. 1104.
11. Sorbie, K. S., and Liang, N. , *How Scale Inhibitors Work: Mechanisms of Selected Barium Sulphate Scale Inhibitors Across a Wide Temperature Range.* Society of Petroleum Engineers, 2004. SPE 87470.
12. Boak, L. S., Graham, G. M., Sorbie, K. S., *The Influence of Divalent Cations on the Performance of $BaSO_4$ Scale Inhibitor Species.* The Society of Petroleum Engineers, 1999. 50771(SPE International Symposium on Oilfield Chemistry, Houston TX).
13. Cook, B.C., *Characterization of Comb Polymer Kypam for Enchanced Oil Recovery*, in *Chemical & Petroleum Engineering*. 2006, University of Kansas: Lawrence, KS. p. 145.
14. Graham, G. M., Sorbie, K. S. and Jordan, M. M., *How Scale Inhibitors Work and How This Affects Test Methodology*, in *IBC Ltd. Conference "Solving Oilfield Scaling"*. 1997: Aberdeen, UK.
15. Sorbie, K. S. and Gdanski, R. D., *A complete Theory of Scale-Inhibitor Transport and Adsorption/Desorption in Squeeze Treatments.* Society of Petroleum Engineers, 2005 (SPE 95088). Richardson, TX
16. Shields, R. A., Sorbie, K. S. and Singleton, M. A., *Analysis of the Mechanism of Transport and Retention of Nonaqueous-Scale-Inhibitor Treatmetns in Cores Using Novel Tracer Techniques.* Society of Petroleum Engineers, 2008. (SPE 100518)
17. Fan, C., Kan A. T. and Tomson M., *Barite Nucleation and Inhibition at 0-200^{o}C, With and Without Hydrate Inhibitors*.Society of Petroleum Engineers, 2009 (SPE 121559)
18. Shen, D., Fu, G., Al-Saiari, H., Kan, A. and Tomson, M., S*eawater Injection, Inhibitor Transport, Rock-Brine Interaction, and $BaSO_4$ Scale Control During Seawater Injection.* Societpy of Petroleum Engineers, 2008 (SPE 114062)

19. Graham, G.M., Boak, L. S., and Sorbie, K.S., *The Influence of Formation Calcium and Magnesium on the Effectiveness of Generically Different Barium Sulphate Oilfield Scale Inhibitors*. Society of Petroleum Engineers, 2003 (SPE 81825)
20. Balastre, M., Persello, J., Foissy, A. and Argillier, J F., *Binding and Ion-Exchange Analysis in the Process of Adsorption of Anionic Polyelectrolytes on Barium Sulphate*. Journal of Colloid and Interface Science, 1999 (p. 299)
21. Sorbie, K. S., Yuan, M. D., Chen, P., Todd, A. C. and Wat, R. M. S., *The Effect of pH on the Adsorption and Transport of Phosphonate Scale Inhibitor Through Porous Media.* Society of Petroleum Engineers, 1993. Presented at the SPE International Symposium on Oilfield Chemistry, New Orleans.
22. Yuan, M. D., Jamieson, E. and Hammonds, P., *Investigation of Scaling and Inhibition Mechanisms and the Influencing Factors in Static and Dynamic Inhibition Tests*. Paper No 98067 Presented at the NACE Annual Conference and Exposition in San Diego, CA. March, 1998.
23. Sorbie, K. S., Jiang, P., Yuan, M. D., Chen, P., Jordan, M. M. and Todd, A. C., *The Effect of pH, Calcium and Temperature on the Adsorption of Phosphonate Inhibitors Onto Consolidated and Crushed Sandstone*. Society of Petroleum Engineers, 1993 (SPE 26605). Houston, TX.
24. Braley, N. J., Brunt, D. C., Payne, G. E. and Wofl, N.O., *Evaluation of Scale Inhibitors for Downhole Squeeze Treatment*. Societly of Petroleum Engineers, 1991. (SPE 23108)
25. Romero, C., Bazin, B., Zaitoun, A. and Leal-Calderon, F., *Behavior of a Scale Inhibitor Water-in-Oil Emulsion in Porous Media*. Society of Petroleum Engineers, 2007. (SPE 98275)

Appendix A

pH Results

The following are the results of the pH data acquired in the displacement experiments. The sampling was performed for selected vials that were used for concentration measurements afterwards.

Table A. 1 5% SI in RO water Displaced by FB Experiment pH Results

Sample #	PV	pH	Sample #	PV	pH
3	0.297	6.5	38	3.495	5.7
5	0.494	6.6	39	3.585	5.9
7	0.666	6.6	40	3.669	5.7
9	0.849	6.7	41	3.735	5.3
10	0.944	6.7	42	3.828	5.5
11	1.035	6.6	43	3.924	5.7
12	1.127	5.0	44	4.020	5.9
13	1.220	5.2	45	4.116	5.7
14	1.314	5.7	46	4.214	5.3
15	1.407	5.7	47	4.310	4.4
16	1.500	5.7	48	4.407	4.4
17	1.593	5.7	49	4.503	4.4
18	1.685	5.7	50	4.600	4.4
19	1.777	5.7	51	4.696	4.4
20	1.868	5.9	52	4.794	4.4
24	2.232	5.9	54	4.992	4.6
26	2.413	5.9	55	5.090	4.9
28	2.595	5.9	58	5.385	5.7
30	2.775	6.0	60	5.583	6.1
31	2.866	6.0	70	6.566	6.4
32	2.957	6.0	75	7.059	6.3
33	3.046	6.0	80	7.551	6.4
34	3.136	6.0	85	8.043	6.4
36	3.316	5.9	90	8.537	6.3
37	3.405	5.3	100	9.525	6.3

Table A. 2 5% SI in SW Displaced by FB Experiment pH Results

Sample #	PV	pH	Sample #	PV	pH
3	0.291	6.3	38	3.748	4.1
5	0.488	6.5	40	3.95	4.1
8	0.781	6.1	42	4.153	4.1
9	0.879	6.3	43	4.254	4.2
10	0.978	5.6	44	4.354	4.1
11	1.076	5	45	4.454	4.1
12	1.174	4.4	46	4.553	4.2
13	1.273	4.1	47	4.653	4.1
15	1.47	4.2	48	4.752	4.1
17	1.667	4.1	50	4.95	4.2
20	1.961	4.1	53	5.248	4.2
23	2.257	4.1	56	5.548	4.3
26	2.553	4.1	60	5.948	4.8
28	2.751	4.2	65	6.442	5.9
30	2.948	4.1	70	6.941	5.9
31	3.047	4.1	75	7.441	6.3
32	3.146	4.1	80	7.943	6.4
33	3.249	4.1	85	8.442	6.3
34	3.347	4.1	90	8.943	6.5
36	3.548	4.1	100	9.95	6.6

Table A. 3 SW Displaced by FB Experiment pH Results

Sample #	PV	pH
3	0.310	6.7
5	0.518	6.8
8	0.831	6.9
10	1.039	6.7
11	1.143	6.6
13	1.352	6.5
15	1.561	6.5
18	1.874	6.5
22	2.290	6.5
25	2.600	6.3
28	2.911	6.3
33	3.331	6.1
37	3.729	5.9
40	4.029	5.7
42	4.228	5.9
43	4.327	5.9
44	4.426	5.7
45	4.525	5.7
46	4.624	5.6
47	4.722	5.7
48	4.822	5.6
49	4.921	5.6
50	5.019	5.7
53	5.316	6.1
55	5.514	6.5
60	6.008	6.5
65	6.502	6.7
70	6.999	6.6
75	7.494	6.5
80	7.993	6.5
85	8.492	6.5
90	8.992	6.7
95	9.492	6.6
100	9.996	6.7

Table A. 4 5% SI in RO Water Displaced by RO Water Experiment pH Results

Sample #	PV	pH
3	0.329	5.0
8	0.830	4.9
10	1.032	4.6
11	1.131	4.8
13	1.331	4.8
15	1.530	4.8
17	1.728	5.0
20	2.027	5.0
22	2.223	5.1
25	2.523	5.2
28	2.826	5.2
31	3.035	5.4
34	3.324	5.4
37	3.617	5.6
39	3.813	5.4
42	4.107	5.8
44	4.306	6.1
46	4.500	6.1
48	4.696	6.0
50	4.892	6.0
53	5.188	5.9
56	5.486	5.9
60	5.878	5.0
65	6.370	5.0
70	6.862	4.9

Appendix B

Sand pack Tracer and Pressure Drop Tests

The following plots are the tracer and pressure results from each experiment. The pore volume and permeability were calculated from these results.

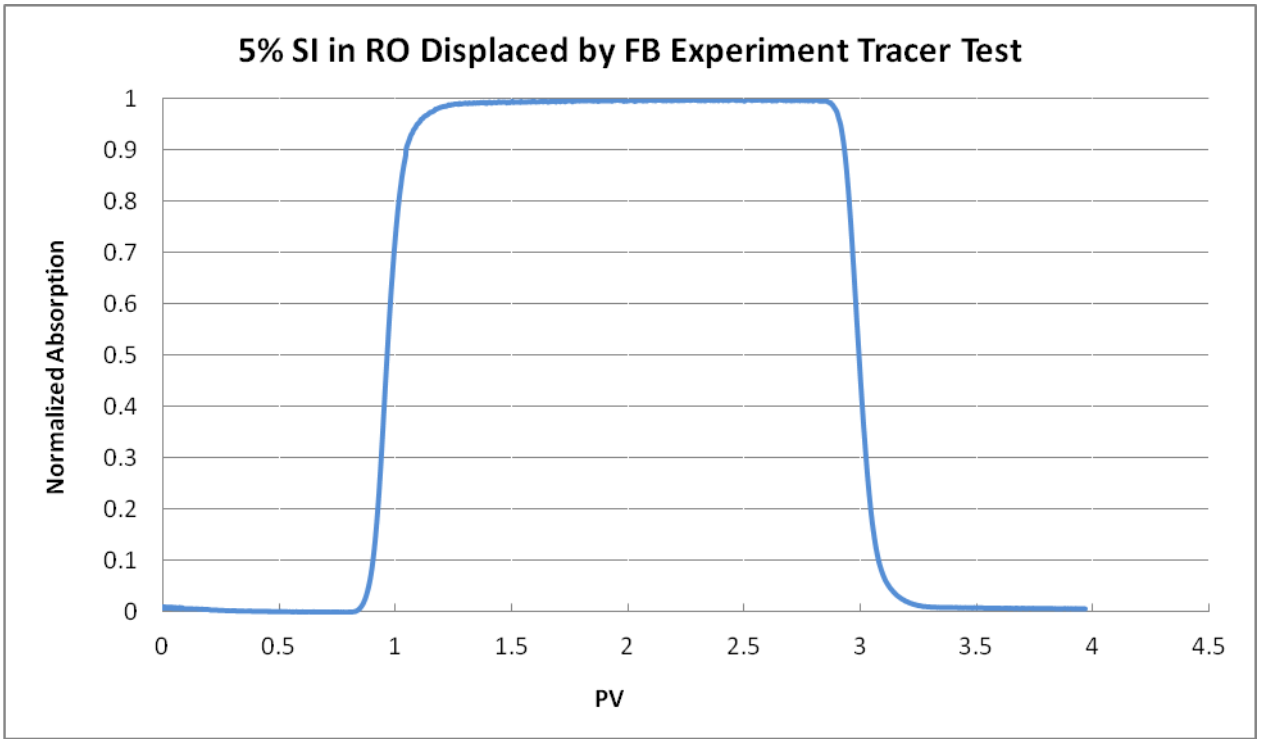

Figure B. 1 Experiment 1 Tracer Test

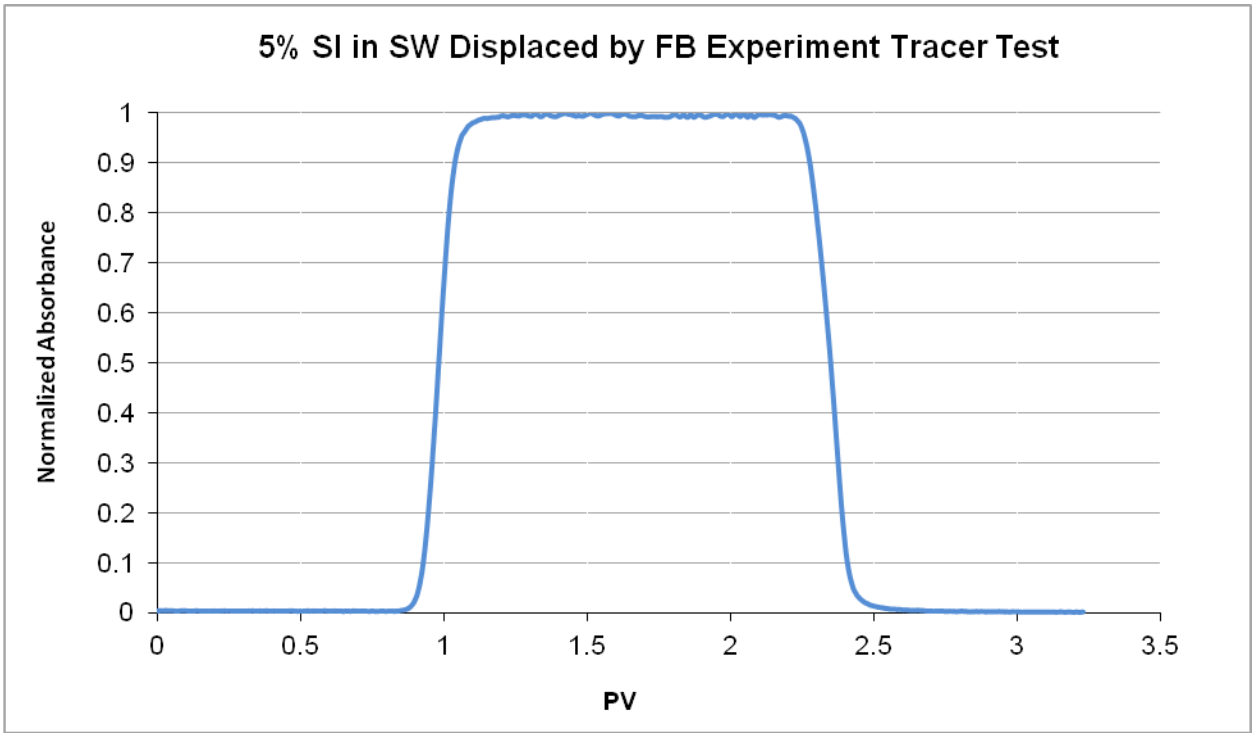

Figure B. 2 Experiment 2 Tracer Test

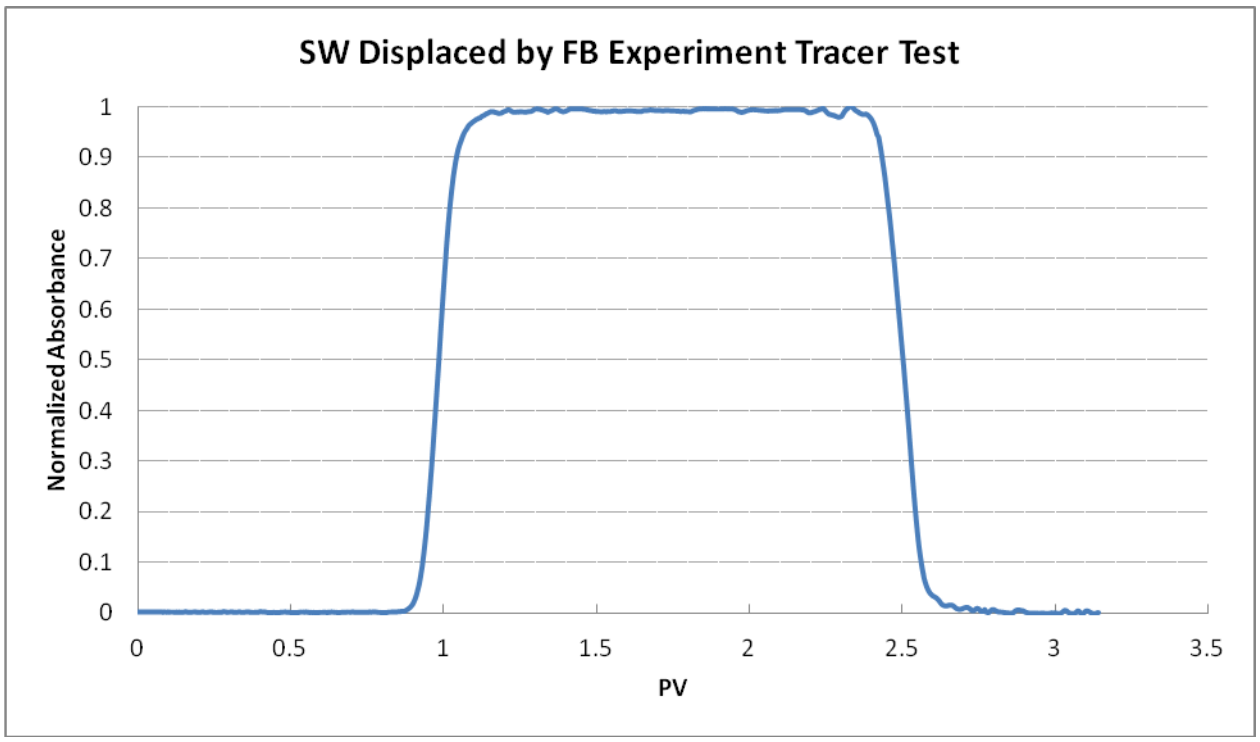

Figure B. 3 Experiment 3 Tracer Test

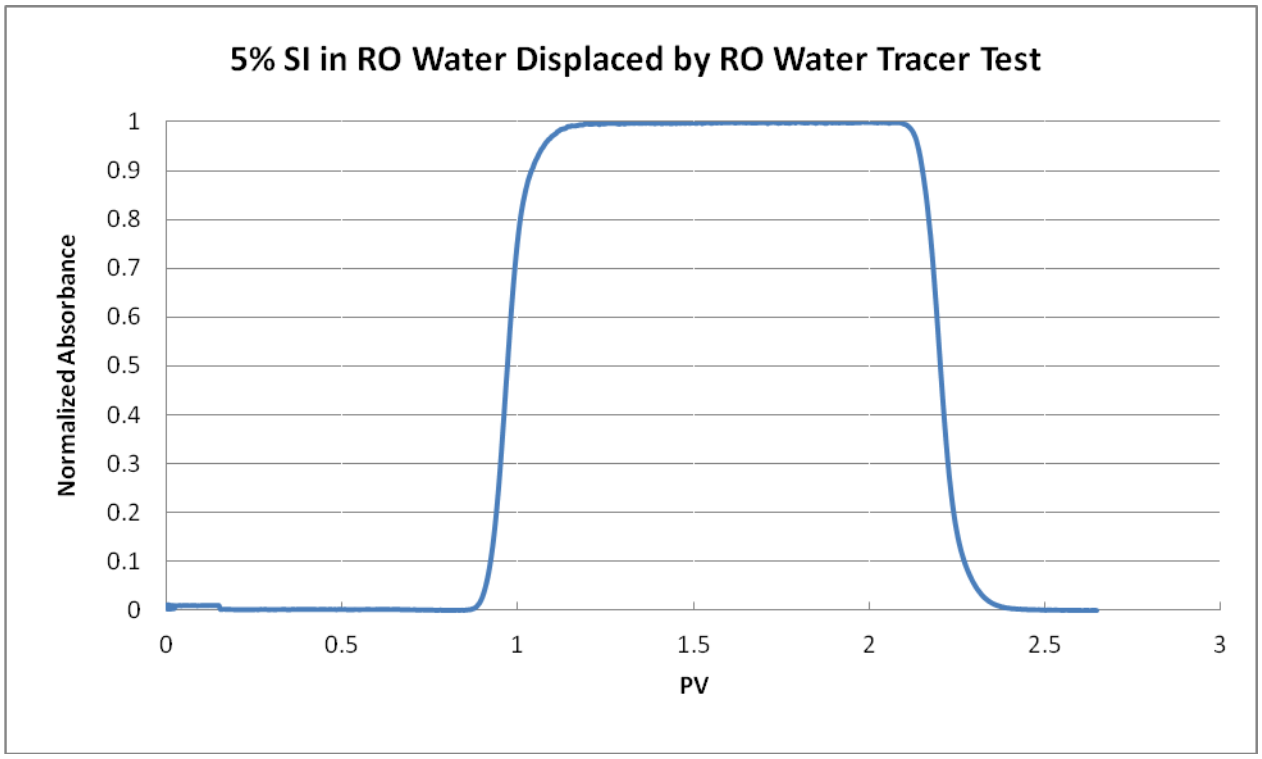

Figure B. 4 Experiment 4 Tracer Test

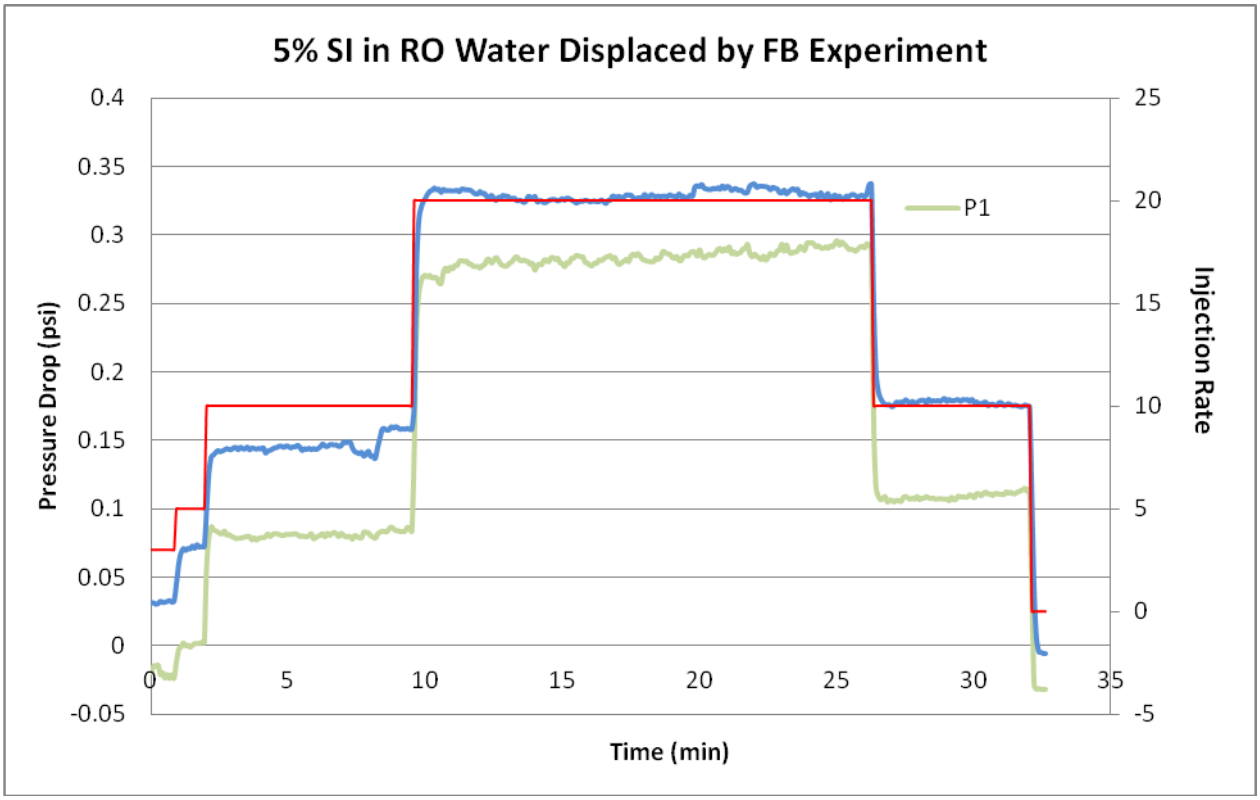

Figure B. 5 Pressure Drop and Injection Rate versus Time Experiment 1

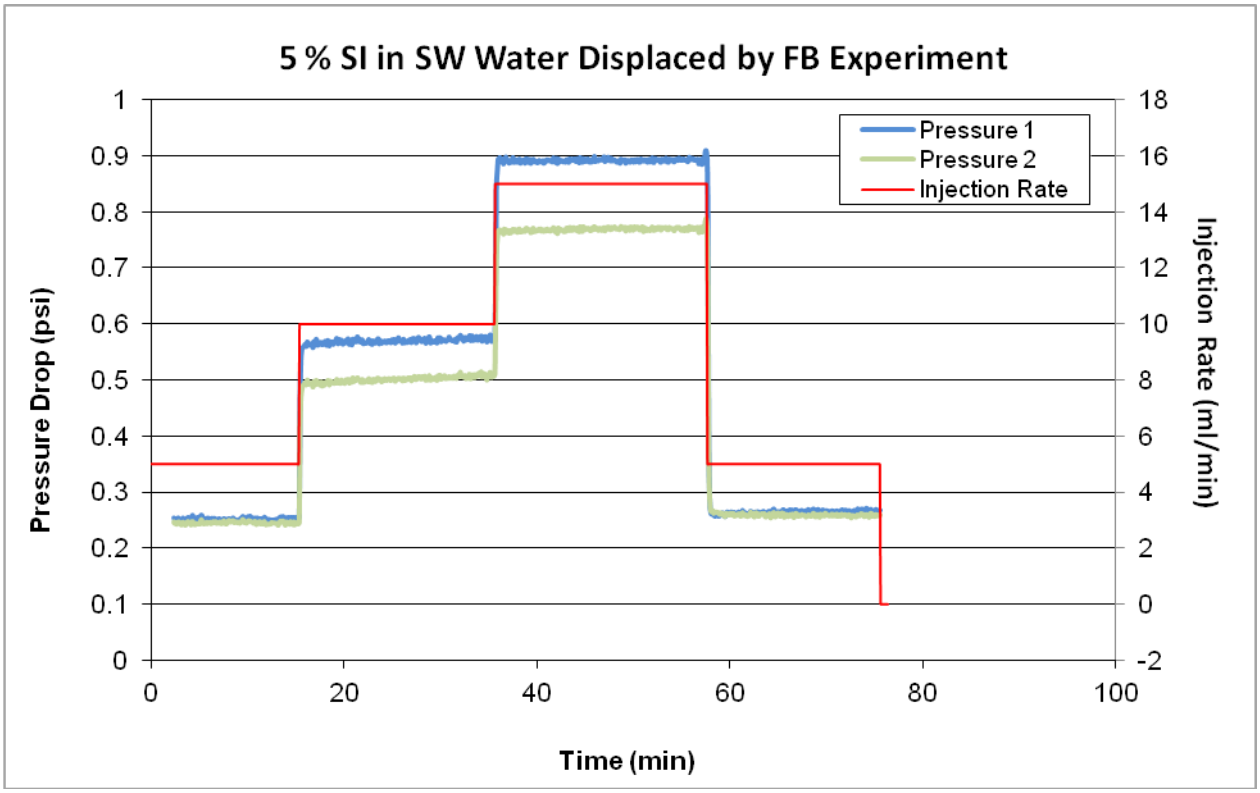

Figure B. 6 Pressure Drop and Injection Rate versus Time Experiment 2

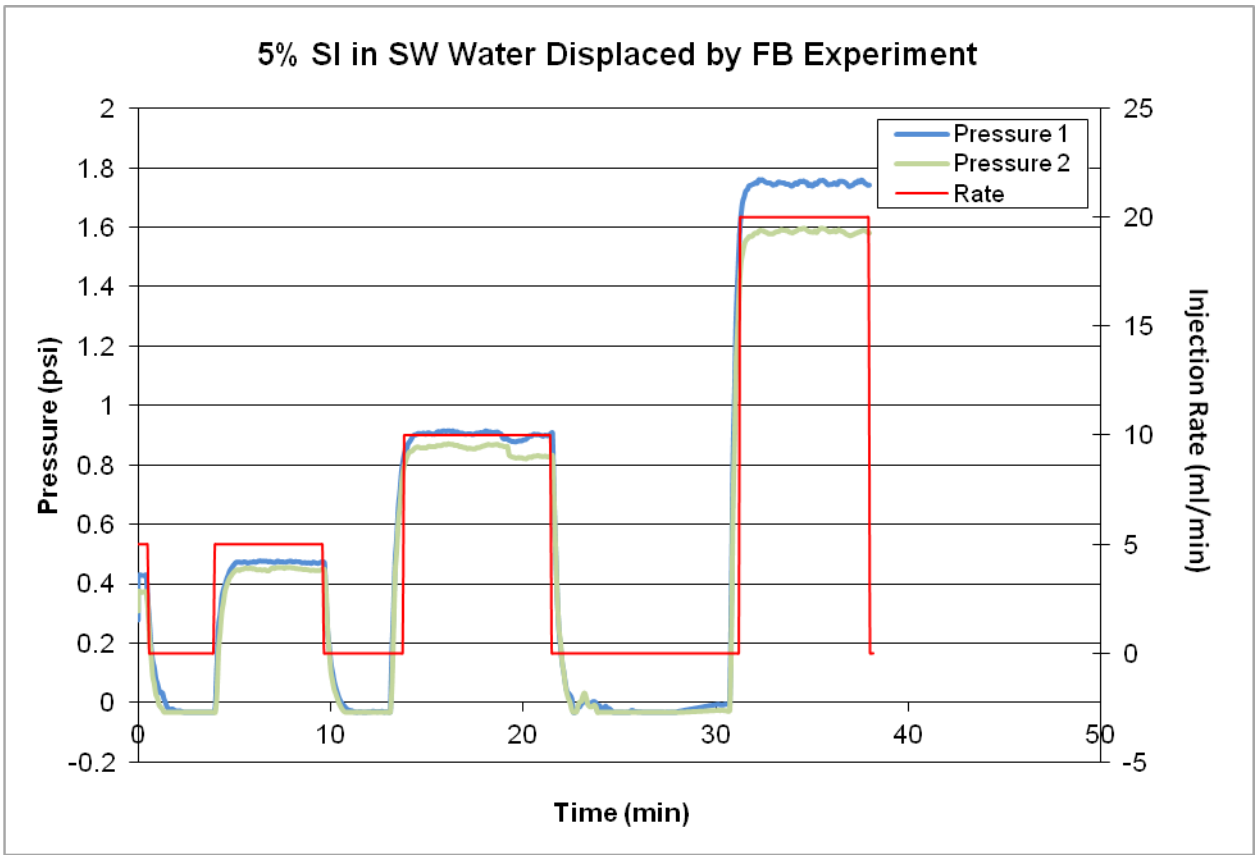

Figure B. 7 Pressure Drop and Injection Rate versus Time Experiment 2

Appendix C

Displacement Experiments Pressure Data

The following plots are the pressure data acquired during the displacement experiments. All pressure transducers were calibrated in advance.

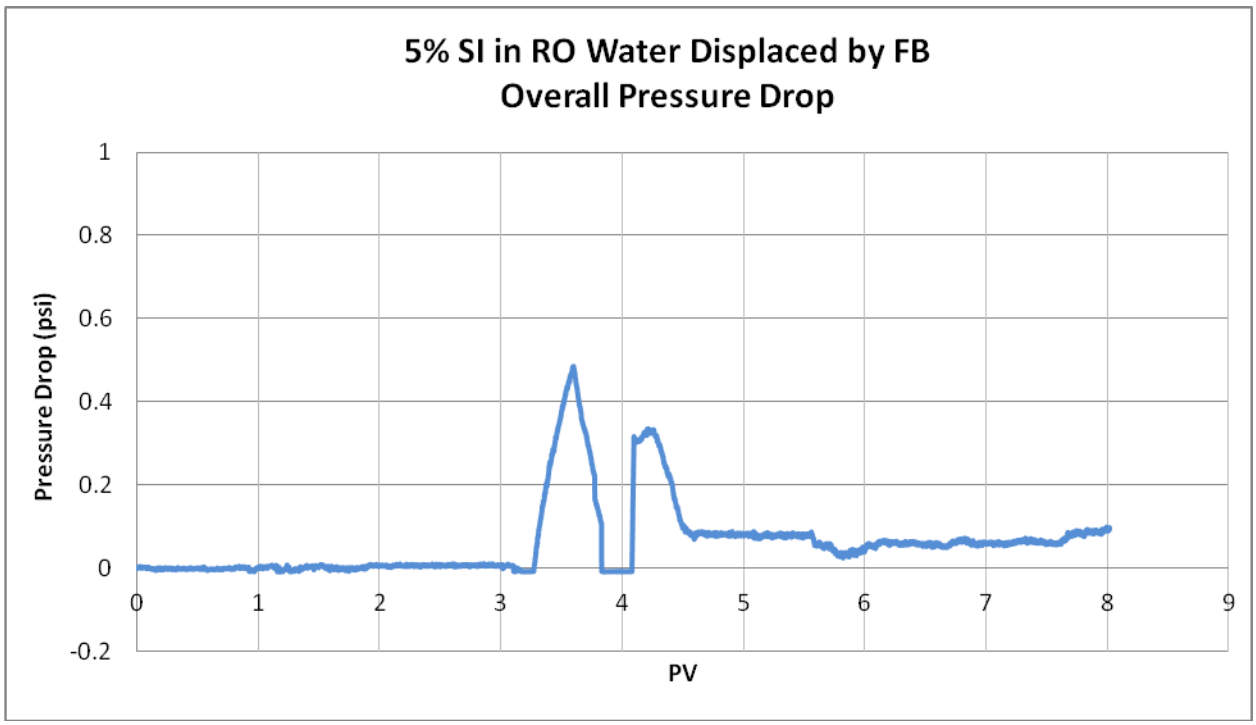

Figure C. 1 Experiment 1 Overall Pressure Drop

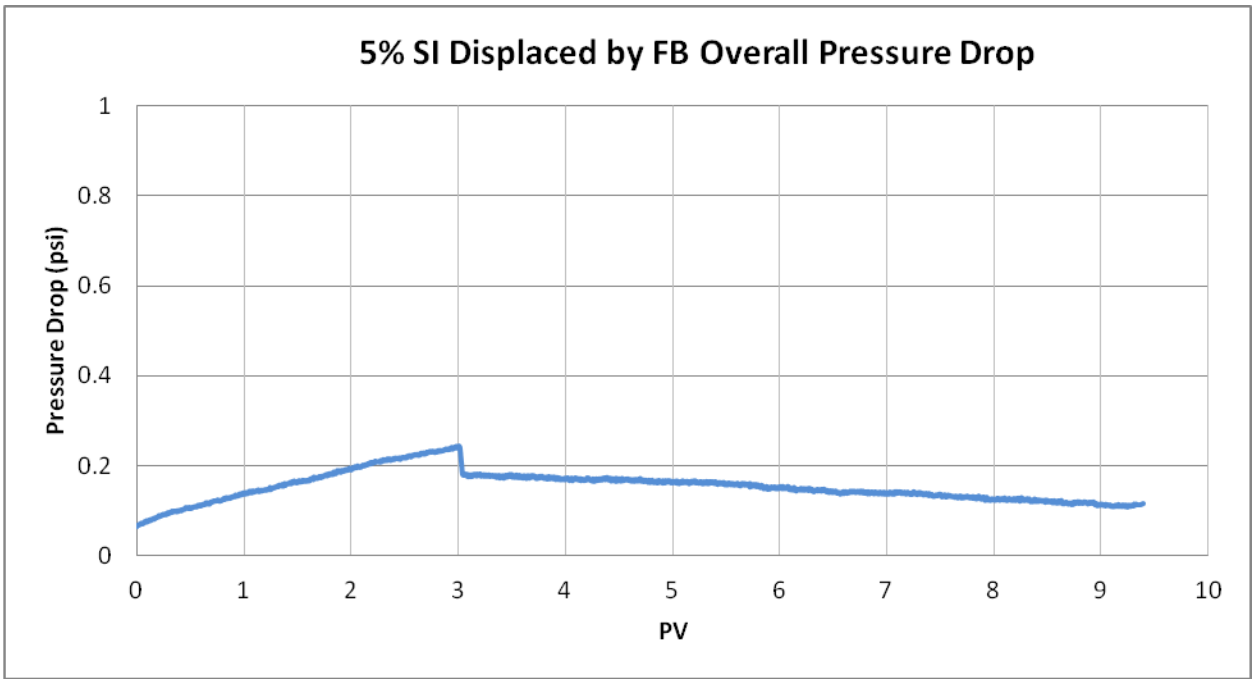

Figure C. 2 Experiment 2 Overall Pressure Drop Data

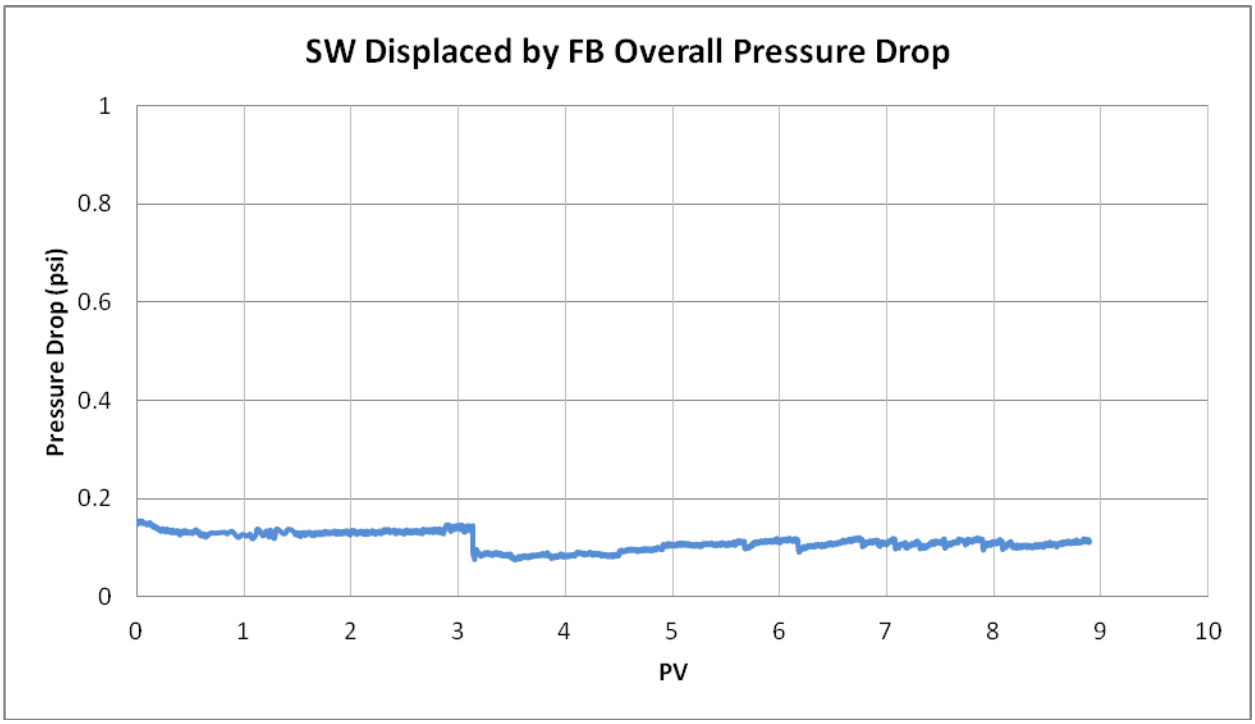

Figure C. 3 Experiment 3 Overall Pressure Drop Data

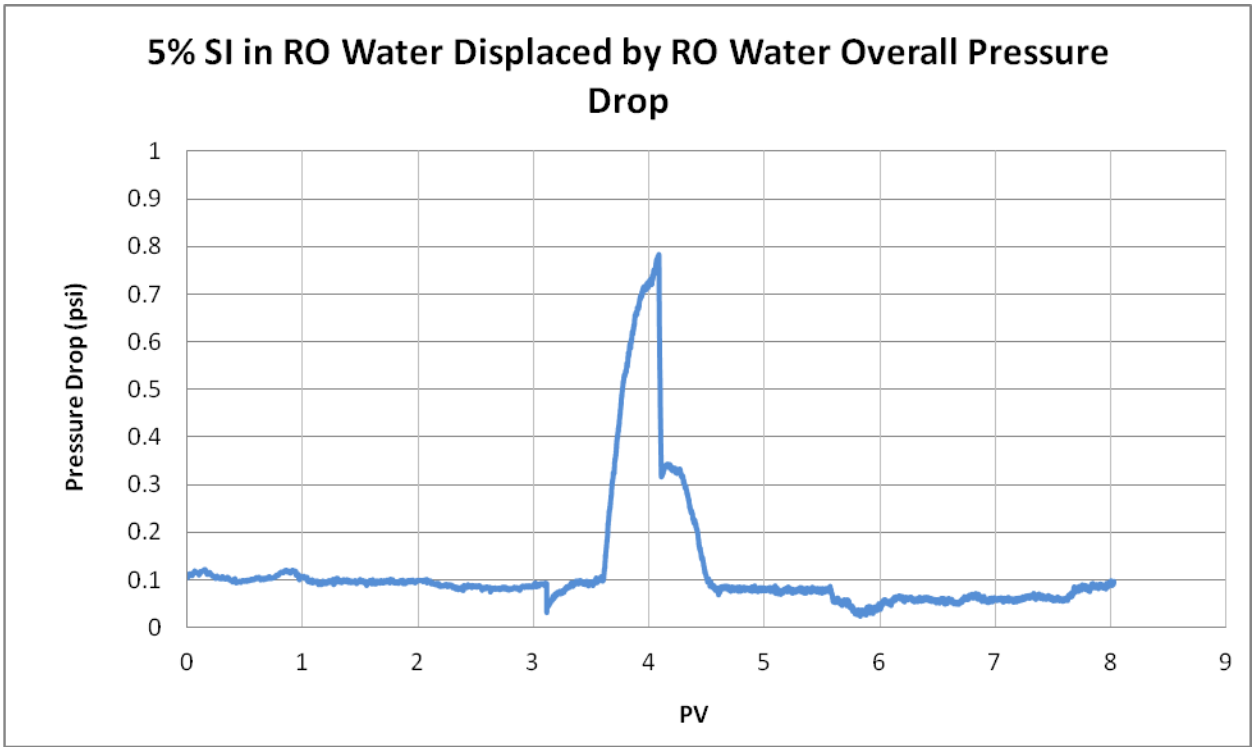

Figure C. 4 Experiment 3 Overall Pressure Drop Data

Appendix D

Dialysis Sulfur Concentration Material Balance

The following calculation was performed by Professor G. Paul Willhite. It was estimated that an average of 85.8 % of sulfur is lost in the dialysis process.

Table D. 1 Dialysis Sulfur Concentration Material Balance (Courtesy of Professor. G. Paul Willhite)

Experiment 1-Retentate(Two Cells)				Experiment 4-used same fluid as Experiment 1	
assumed to be 100% active:					
Ret,g	45.96	pre-dialysis			
Ret Water,g	121.47	pre-dialysis			
Total Sol,g	167.43	pre-dialysis			
Wt fr SI	0.05	Desired			
Makeup RO Water, g	797.73				
Total Sol, g	965.16				
Wt fr SI	0.047619	actual			
	0.002381				
Ret, g	167.43				
Makeup RO	797.73				
Total,g	965.16				
S, ppm	218	From ICP		S, ppm	225
S, g	0.210			S, g	0.225
S, retentate	1257				
S, g/g	0.000218			S, g/g	0.000225
S, wt%	0.0218			S, wt%	0.0225
SI original,g	45.96			SI original,g	45.96
Wt frac S-orig	0.004578	after dialysis		Wt frac S-orig	0.004896
Wt frac S-orig	0.0328			Wt frac S-orig	0.0328
%Loss by dialysis	86.04			%Loss by dialysis	85.07
%-Non dial	13.96			%-Non dial	14.93

Experiment 2-Used One Cassette					
Ret, g	25.08	pre-dialysis			
Ret Water,g	69.81	pre-dialysis			
Total Sol	94.89	pre-dialysis			
Mixed 94.89 grams with SW				S, ppm	S, g
Makeup SW	431.79		SW,g	1028	0.444
Total Sol	526.68		SI+SW	1057	0.557
S from SI,g					0.113
S from SI,ppm					214
S, orig solution after dialysis and dilution, wt fr					0.004498
S, retentate, ppm					1189
Wt frac S-orig	0.0328	from Sheng-Xue's analysis			
Loss by dialysis, wt fraction			0.0283		
% Loss by dialysis			86.3		
%-Non dial			13.7		

Appendix E

Pore Volume Correction to Collected Vials for ICP Analysis

Each collected sample's volume was approximately 10 ml and since the ICP analysis was performed for the whole sample, a determination of pore volume corresponding to concentration was needed. Therefore, the mid- point for each vials' volume is considered as the PV corresponding to the ICP concentration results. The correction was performed using the following formula:

$$PV_{corrected} = PV_{Actual} - \frac{\left(\frac{Vial\ Volume}{2}\right)}{Sandpack\ PV}$$

Table E. 1 Experiment 1 PV corrections

Sample #	PV	PV Corrected	S (mg/L)	Ca (mg/L)	Mg (mg/L)	Ba (mg/L)	Sr (mg/L)	Si (mg/L)
Alpine Brine			5.71	141.58	92.9	55.7	14.1	0.280
Scale Inhibitor			218	0.710	0.283	0.0597	0.0249	0.590
3	0.297	0.248	7.08	142.1	93.9	56.2	14.2	0.998
6	0.574	0.525	5.59	145.6	93.9	57.2	14.4	1.82
9	0.849	0.800	5.67	142.1	92.9	56.2	13.9	2.69
10	0.944	0.895	5.48	146.1	95.9	57.7	14.5	3.03
11	1.035	0.986	10.9	144.5	95.8	57.4	14.4	3.30
12	1.127	1.078	217	101.2	64.2	44.6	10.0	6.69
13	1.220	1.171	400	5.19	6.88	4.60	1.12	5.62
14	1.314	1.265	373	5.19	6.88	4.60	1.12	4.59
15	1.407	1.358	351	2.77	4.61	2.93	0.750	4.05
16	1.500	1.451	322	3.08	4.29	2.44	0.695	4.34
17	1.593	1.544	310	2.68	3.96	2.01	0.674	3.69
20	1.868	1.819	284	1.15	2.13	0.899	0.382	3.81
22	2.051	2.002	281	0.989	1.70	0.725	0.308	4.15
25	2.323	2.274	282	0.749	1.23	0.550	0.218	4.26
28	2.595	2.546	271	0.664	1.03	0.524	0.186	3.90
30	2.775	2.726	267	0.617	0.93	0.513	0.165	3.47
31	2.866	2.817	276	0.743	0.91	0.548	0.170	4.00
34	3.136	3.087	274	0.682	0.80	0.500	0.142	3.17
37	3.405	3.356	274	10.3	7.58	6.73	1.23	10.6
39	3.585	3.536	262	1.25	2.43	1.44	0.547	10.2
42	3.828	3.779	271	3.69	3.77	2.35	0.700	11.0
44	4.020	3.971	247	1.63	2.75	1.71	0.536	11.0
45	4.116	4.067	256	3.85	3.75	2.11	0.650	10.5
46	4.214	4.165	224	5.88	4.88	2.46	0.689	9.78
47	4.310	4.261	104	77.4	53.1	27.8	7.84	8.47
48	4.407	4.358	31.3	134	86.1	50.5	13.1	4.33
50	4.600	4.551	16.3	150	97.3	57.4	14.6	5.61
53	4.893	4.844	12.1	151	99.0	58.5	15.1	2.25
56	5.188	5.139	15.0	151	99.1	58.4	14.8	2.33
59	5.484	5.435	15.6	143	96.3	57.2	14.7	2.29
64	5.975	5.926	3.58	147	98.0	57.2	14.88	2.08

Table E. 2 Experiment 2 PV corrections

SandPack 2	PV	PV Corrected	S	Ca	Mg	Ba	Sr	Si
5% ST852 in SW			1057	349	1740	0.0500	0.220	3.06
Alpine Brine			6.5	146	97	58.1	15.0	0.422
Sea Water			1028	407	2030	0.0400	0.220	2.99
3	0.291	0.241	14.4	157	105	62.7	16.1	96.7
5	0.488	0.437	12.1	165	111	65.9	16.8	103
8	0.781	0.730	8.25	155	104	62.4	15.9	34.7
9	0.879	0.829	7.51	153	102	60.8	15.5	20.8
10	0.978	0.927	10.4	151	103	59.9	15.4	18.9
11	1.076	1.025	303	208	558	38.7	1.88	18.4
12	1.174	1.124	853	323	1500	11.5	3.27	10.4
13	1.273	1.223	992	345	1690	3.64	1.03	7.34
14	1.372	1.321	1034	352	1760	1.37	0.390	6.22
15	1.470	1.419	966	345	1740	0.700	0.270	5.44
17	1.667	1.617	990	345	1730	0.480	0.250	5.06
20	1.961	1.911	1034	351	1770	0.400	0.250	4.83
23	2.257	2.206	1028	355	1800	0.360	0.240	4.63
26	2.553	2.502	1044	359	1800	0.340	0.240	4.36
28	2.751	2.700	1039	363	1830	0.330	0.240	4.21
30	2.948	2.898	1057	344	1750	0.300	0.230	4.14
31	3.047	2.997	998	363	1800	0.310	0.240	3.84
32	3.146	3.096	1028	354	1790	0.300	0.230	3.86
33	3.249	3.198	1071	360	1790	0.390	0.280	18.1
34	3.347	3.296	1014	359	1790	0.350	0.260	24.8
36	3.548	3.497		359	1790	0.350	0.260	
38	3.748	3.698	1080	357	1780	0.370	0.300	29.8
40	3.950	3.900	1061	357	1770	0.290	0.260	29.8
42	4.153	4.103	1005	337	1650	1.10	0.930	23.8
43	4.254	4.204	426	227	762	26.0	8.33	11.3
44	4.354	4.304	136	172	298	49.2	13.2	8.17
45	4.454	4.404	41.6	158	154	57.4	15.1	8.75
46	4.553	4.503	13.2	152	108	59.7	15.4	10.5
47	4.653	4.602	10.6	151	103	59.5	15.5	12.4
48	4.752	4.701	10.4	155	108	61.9	15.9	14.3
50	4.950	4.900	9.74	154	104	60.9	15.7	16.7
53	5.248	5.198	10.3	153	102	60.4	15.7	19.0
56	5.548	5.498	10.2	153	102	60.6	15.6	19.7
60	5.948	5.898	10.8	155	103	61.6	15.8	18.9
65	6.442	6.392	12.1	153	102	61.3	15.6	16.8
70	6.941	6.891	10.9	153	101	60.7	15.6	14.2
75	7.441	7.390	10.8	150	99.9	60.1	15.4	11.8

Table E. 3 Experiment 3 PV corrections

SandPack 3	PV	PV Corrected	S	Ca	Mg	Ba	Sr	Si
Alpine Brine			3.22	149	102	57.9	14.6	0.0740
Sea Water			1052	413	2020	0.100	0.170	1.84
3	0.310	0.261	5.09	145	96.5	57.6	14.4	23.9
5	0.518	0.469	5.96	147	96.9	57.4	14.4	22.5
8	0.831	0.782	5.49	145	95.4	57.3	14.4	18.2
10	1.039	0.990	148	181	315	1.69	10.7	18.5
11	1.143	1.094	860	361	1640	0.430	3.13	15.9
13	1.352	1.303	1061	395	1940	0.470	0.120	12.7
15	1.561	1.512	1070	414	2030	0.350	0.090	10.5
18	1.874	1.825	1070	412	2010	0.270	0.080	8.51
22	2.290	2.241	1079	419	2090	0.230	0.070	6.74
25	2.600	2.551	1061	416	2090	0.210	0.070	6.06
28	2.911	2.862	1039	415	2070	0.420	0.200	5.76
33	3.331	3.282	1074	430	2140	0.140	0.110	25.1
37	3.729	3.680	1074	425	2140	0.120	0.110	23.5
40	4.029	3.980	1082	427	2110	0.110	0.100	26.1
42	4.228	4.179	291	222	661	0.340	8.05	12.0
43	4.327	4.278	38.3	160	187	2.18	11.8	6.60
44	4.426	4.377	8.66	153	109	51.8	14.9	5.39
45	4.525	4.476	7.70	153	103	56.8	14.9	5.40
46	4.624	4.575	6.24	130	88.0	49.4	12.8	5.41
47	4.722	4.673	6.42	148	100	56.4	14.6	5.27
48	4.822	4.773	6.64	150	102	57.5	14.9	5.52
49	4.921	4.872	7.77	150	101	57.5	14.8	5.66
50	5.019	4.970	7.92	148	100	57.1	14.7	5.76
53	5.316	5.267	7.37	151	100	57.9	14.8	5.75
55	5.514	5.465	8.08	148	98.6	57.4	14.7	5.61
60	6.008	5.959	8.68	149	98.9	57.4	14.7	5.10
65	6.502	6.453	8.92	146	97.3	56.5	14.5	4.54
70	6.999	6.950	8.19	150	101	57.7	14.8	4.26
75	7.494	7.445	9.17	149	100	57.4	14.9	3.85

Table E. 4 Experiment 4 PV corrections

SandPack 4	PV	PV Corrected	S (mg/L)	Si (mg/L)
SI in RO water			225	0
3	0.329	0.281	10.2	0
8	0.830	0.782	11.0	0
10	1.032	0.984	124	5.82
11	1.131	1.083	263	8.01
12	1.231	1.183	282	8.85
13	1.331	1.283	273	10.2
15	1.530	1.482	282	12.9
17	1.728	1.680	264	15.7
20	2.027	1.978	240	22.4
22	2.223	2.175	250	42.2
25	2.523	2.475	247	107
28	2.826	2.778	243	176
31	3.035	2.987	250	225
34	3.324	3.276	243	144
37	3.617	3.569	237	126
39	3.813	3.765	249	150
42	4.107	4.059	35.1	139
43	4.205	4.157	20.0	111
44	4.306	4.258	14.7	113
45	4.402	4.354	12.3	109
46	4.500	4.452	11.3	87.1
47	4.600	4.552	10.6	81.0
48	4.696	4.648	10.5	79.5
49	4.794	4.746	10.5	74.9
50	4.892	4.844	10.4	62.1
53	5.188	5.140	10.0	40.3
56	5.486	5.438	9.92	36.5
60	5.878	5.830	10.1	31.0
65	6.370	6.322	9.95	25.0
68	6.667	6.619	10.0	19.8